

Constraining the interaction strength between dark matter and visible matter: I. fermionic dark matter

Jia-Ming Zheng¹, Zhao-Huan Yu^{1,2}, Jun-Wen Shao¹, Xiao-Jun Bi², Zhibing Li¹, and Hong-Hao Zhang^{1*}

¹*School of Physics and Engineering, Sun Yat-Sen University, Guangzhou 510275, China*

²*Key Laboratory of Particle Astrophysics, Institute of High Energy Physics, Chinese Academy of Sciences, Beijing 100049, China*

In this work we study the constraints on the dark matter interaction with the standard model particles, from the observations of dark matter relic density, the direct detection experiments of CDMS and XENON, and the indirect detection of the \bar{p}/p ratio by PAMELA. A model independent way is adopted in the study by constructing the effective interaction operators between dark matter and standard model particles. The most general 4-fermion operators are investigated. We find that the constraints from different observations are complementary with each other. Especially the spin independent scattering gives very strong constraints for corresponding operators. In some cases the indirect detection of \bar{p}/p data can actually be more sensitive than the direct detection or relic density for light dark matter ($\lesssim 70$ GeV).

PACS numbers: 95.35.+d, 95.30.Cq, 95.85.Ry

I. INTRODUCTION

The existence of a significant component of nonbaryonic dark matter (DM) in the Universe has been well confirmed by astrophysical observations [1–3] in recent years, however the nature of this substance remains unclear. Since there is no candidate for DM in the Standard Model (SM) of particle physics, it implies the existence of new physics beyond the SM. Probe of the microscopic identity and properties of DM has become one of the key problems in particle physics and cosmology (for reviews of DM, see, for instance, [4–8]).

Among a large amount of theoretical models, a well-motivated candidate for DM is the weakly interacting massive particle (WIMP). This WIMP must be stable, nonrelativistic, electrically neutral, and colorless. If the mass of WIMP is from a few GeV to TeV and the interaction strength is of the weak scale, they can naturally yield the observed relic density of DM, which is often referred to as the WIMP miracle [8]. A huge variety of new physics models trying to solve the problems of the SM at the weak scale can naturally contain WIMP candidates, such as the supersymmetric models [5, 9–11], extra dimensional models [12–19], little Higgs models [20–24], left-right symmetric models [25–28], and many other theoretical scenarios.

The above mentioned specific models are well-motivated, however they still lack experimental support. We do not know whether nature really behaves like one of them or some other yet unconsidered theories. Moreover, in case the DM particle is the only new particle within the reach of LHC and other new particle species are much heavier than DM, it will be very difficult to tell which model the DM particle belongs to. Additionally, it is possible that the DM may be first observed by direct or indirect detection experiments. These early observations may only provide information about some general properties of the DM particle, and may not be able to distinguish the underlying theories. Therefore, the model-independent studies of the DM phenomenology are particularly important for they may avoid theoretical bias [29–34]. Recently there have been quite a few papers following such consideration and adopting a model-independent way to study various phenomenologies related with DM [35–43]. Especially the relic density measured by WMAP [3], direct detection from CDMS [44], XENON [45] and possible collider signals from LHC are considered in these studies.

In this work, we first construct the general effective 4-fermion interaction operators between DM particles and the SM particles, which extend the effective fermionic WIMP interactions given in Ref. [32]. Here we focus on Dirac fermionic DM. Discussions on scalar and vector DM will be presented in companion papers. We then give updated constraints from the DM relic density within the 7-year WMAP data [3] and the spin-independent WIMP-nucleus elastic scattering searches by CDMS II [44] and XENON100 [45], and compare our results with those in Ref. [32]. In addition, we present new phenomenological constraints on these effective models from the spin-dependent WIMP-nucleus elastic scattering searches by CDMS [46] and XENON [47] and the cosmic-ray antiproton-to-proton ratio by PAMELA [58]. We find that the constraints from different kinds of experiments are rather comparable. Combination of these constraints provides more information of the effective models.

* Email: zhh98@mail.sysu.edu.cn

This paper is organized as follows. In Sec. II we briefly describe the effective DM models of various 4-fermion interaction operators. In Sec. III, IV and V we explore the constraints on these models from the DM relic density, direct and indirect detection searches, respectively. In Sec. VI we discuss the validity region of effective theory and present the combined constraints on the effective coupling constants of these models. Sec. VII is the conclusion.

II. EFFECTIVE MODELS

We start with the case that DM is a single Dirac fermionic WIMP (χ). Instead of considering a WIMP candidate from a specific theoretical model, we study the phenomenologies in a model-independent way by constructing effective interaction operators between χ and the SM particles. These interaction operators are constrained only by the requirements of Hermiticity, Lorentz invariance and CPT invariance.

To proceed, we make the following assumptions similar to those in Ref. [32]: (1) The WIMP is the only new particle at the electroweak scale, and any new particle species other than the WIMP has a mass much larger than the WIMP. This implies that the WIMP's thermal relic density is not affected by resonances or coannihilations, and this makes it possible to describe the interaction between the WIMPs and the standard model particles in terms of an effective field theory. (2) The WIMP only interacts with the standard model fermions through a 4-fermion effective interaction, but not with other particles like gauge or Higgs bosons. This 4-fermion effective interaction is assumed to be dominated by only one form (scalar, vector, etc.) of the set of 4-fermion operators for simplicity. (3) The WIMP annihilation channels to the standard model fermion-antifermion pairs dominate over other possible channels. In other words, the possible channels to final states that include gauge or Higgs bosons are assumed to be negligible for simplicity. However, it should be noted that the supersymmetric DM model actually cannot satisfy the three assumptions above simultaneously in order to give the correct relic density. Even so these assumptions are still useful for a general research.

The effective Lagrangian between two fermionic WIMPs (χ and $\bar{\chi}$) and two standard model fermions (f and \bar{f}) is given by only one of the following expressions:

$$\text{Scalar interaction (S)} : \quad \mathcal{L}_S = \sum_f \frac{G_{S,f}}{\sqrt{2}} \bar{\chi} \chi \bar{f} f \quad (1)$$

$$\text{Pseudoscalar interaction (P)} : \quad \mathcal{L}_P = \sum_f \frac{G_{P,f}}{\sqrt{2}} \bar{\chi} \gamma_5 \chi \bar{f} \gamma_5 f \quad (2)$$

$$\text{Vector interaction (V)} : \quad \mathcal{L}_V = \sum_f \frac{G_{V,f}}{\sqrt{2}} \bar{\chi} \gamma^\mu \chi \bar{f} \gamma_\mu f \quad (3)$$

$$\text{Axialvector interaction (A)} : \quad \mathcal{L}_A = \sum_f \frac{G_{A,f}}{\sqrt{2}} \bar{\chi} \gamma^\mu \gamma_5 \chi \bar{f} \gamma_\mu \gamma_5 f \quad (4)$$

$$\text{Tensor interaction (T)} : \quad \mathcal{L}_T = \sum_f \frac{G_{T,f}}{\sqrt{2}} \bar{\chi} \sigma^{\mu\nu} \chi \bar{f} \sigma_{\mu\nu} f \quad (5)$$

$$\text{Scalar-pseudoscalar interaction (SP)} : \quad \mathcal{L}_{SP} = \sum_f \frac{G_{SP,f}}{\sqrt{2}} \bar{\chi} \chi \bar{f} i \gamma_5 f \quad (6)$$

$$\text{Pseudoscalar-scalar interaction (PS)} : \quad \mathcal{L}_{PS} = \sum_f \frac{G_{PS,f}}{\sqrt{2}} \bar{\chi} i \gamma_5 \chi \bar{f} f \quad (7)$$

$$\text{Vector-axialvector interaction (VA)} : \quad \mathcal{L}_{VA} = \sum_f \frac{G_{VA,f}}{\sqrt{2}} \bar{\chi} \gamma^\mu \chi \bar{f} \gamma_\mu \gamma_5 f \quad (8)$$

$$\text{Axialvector-vector interaction (AV)} : \quad \mathcal{L}_{AV} = \sum_f \frac{G_{AV,f}}{\sqrt{2}} \bar{\chi} \gamma^\mu \gamma_5 \chi \bar{f} \gamma_\mu f \quad (9)$$

$$\text{Alternative tensor interaction (\tilde{T})} : \quad \mathcal{L}_{\tilde{T}} = \sum_f \frac{\tilde{G}_{T,f}}{\sqrt{2}} \varepsilon^{\mu\nu\rho\sigma} \bar{\chi} \sigma_{\mu\nu} \chi \bar{f} \sigma_{\rho\sigma} f \quad (10)$$

$$\text{Left handed-left handed interaction (LL)} : \quad \mathcal{L}_{LL} = \sum_f \frac{G_{LL,f}}{\sqrt{2}} \bar{\chi} \gamma^\mu (1 - \gamma_5) \chi \bar{f} \gamma_\mu (1 - \gamma_5) f \quad (11)$$

$$\text{Right handed-right handed interaction (RR)} : \quad \mathcal{L}_{\text{RR}} = \sum_f \frac{G_{\text{RR},f}}{\sqrt{2}} \bar{\chi} \gamma^\mu (1 + \gamma_5) \chi \bar{f} \gamma_\mu (1 + \gamma_5) f \quad (12)$$

$$\text{Left handed-right handed interaction (LR)} : \quad \mathcal{L}_{\text{LR}} = \sum_f \frac{G_{\text{LR},f}}{\sqrt{2}} \bar{\chi} \gamma^\mu (1 - \gamma_5) \chi \bar{f} \gamma_\mu (1 + \gamma_5) f \quad (13)$$

$$\text{Right handed-left handed interaction (RL)} : \quad \mathcal{L}_{\text{RL}} = \sum_f \frac{G_{\text{RL},f}}{\sqrt{2}} \bar{\chi} \gamma^\mu (1 + \gamma_5) \chi \bar{f} \gamma_\mu (1 - \gamma_5) f \quad (14)$$

where the sum of f is over all the standard model fermions, and the effective coupling constants G are real numbers which have mass dimension of -2 . The 4 chiral interaction operators, \mathcal{L}_{LL} , \mathcal{L}_{RR} , \mathcal{L}_{LR} and \mathcal{L}_{RL} , are just the combinations of the other operators mentioned above. Here we do not include the interaction operators involving derivative ∂_μ insertions into fermion bilinears, for they have higher momentum dimensions and may be safely ignored in the small momentum limit. Note that the alternative tensor interaction term in (10) has two other equivalent forms, i.e., $\varepsilon^{\mu\nu\rho\sigma} \bar{\chi} \sigma_{\mu\nu} \chi \bar{f} \sigma_{\rho\sigma} f = -2\bar{\chi} \sigma^{\mu\nu} i\gamma_5 \chi \bar{f} \sigma_{\mu\nu} f = -2\bar{\chi} \sigma^{\mu\nu} \chi \bar{f} \sigma_{\mu\nu} i\gamma_5 f$.

Each form of the interaction operators listed above represents an effective model of the WIMP coupled to the standard model fermions. For each case, we can calculate the corresponding annihilation and scattering cross sections, which depend on the WIMP mass M_χ and the coupling constants G_f . Associated with the recent results of the DM relic density, direct and indirect detection experiments, we can obtain the phenomenological constraints on G_f . It would be interesting and meaningful to compare the constraints derived from different experiments.

It is worthwhile to note the symmetry properties of these operators under discrete C, P, and T transformations. The first 5 forms of the operators, \mathcal{L}_{S} , \mathcal{L}_{P} , \mathcal{L}_{V} , \mathcal{L}_{A} and \mathcal{L}_{T} are separately invariant under C, P, and T, while the transformation properties of the other operators are summarized in Table I. The transformation properties of the operators under CP are the same as those under T, given that the coupling constants G are real-valued numbers. Thus, all the operators are actually CPT invariant. If the future experiments indicate that there were some of the C, P, and T symmetries in the DM sector, we may use this table to concentrate on or exclude some interaction operators.

TABLE I. The transformation properties of the 4-fermion operators under C, P, and T. Since \mathcal{L}_{S} , \mathcal{L}_{P} , \mathcal{L}_{V} , \mathcal{L}_{A} and \mathcal{L}_{T} are separately invariant under C, P, and T, they are not listed below. The plus '+' means being invariant under the transformation, while the minus '-' means sign reversal. The transformation properties of the operators under CP are the same as those under T, given that the coupling constants G are real numbers.

	\mathcal{L}_{SP}	\mathcal{L}_{PS}	\mathcal{L}_{VA}	\mathcal{L}_{AV}	\mathcal{L}_{T}	\mathcal{L}_{LL}	\mathcal{L}_{RR}	\mathcal{L}_{LR}	\mathcal{L}_{RL}
P	-	-	-	-	-	\mathcal{L}_{RR}	\mathcal{L}_{LL}	\mathcal{L}_{RL}	\mathcal{L}_{LR}
C	+	+	-	-	+	\mathcal{L}_{RR}	\mathcal{L}_{LL}	\mathcal{L}_{RL}	\mathcal{L}_{LR}
T	-	-	+	+	-	+	+	+	+

III. WIMP ANNIHILATION AND RELIC DENSITY

In order to determine the relic density of WIMPs and the source function of cosmic-ray particles produced by the DM annihilation in the Galaxy, which is relevant to the DM indirect detection, we need to calculate the cross sections of WIMP-antiWIMP annihilation to fermion-antifermion pairs for each case listed in the last section. The result is given by

$$\sigma_{S, \text{ann}} = \frac{1}{16\pi} \sum_f \left(\frac{G_{S,f}}{\sqrt{2}} \right)^2 c_f \sqrt{\frac{s - 4m_f^2}{s - 4M_\chi^2}} \frac{(s - 4M_\chi^2)(s - 4m_f^2)}{s} \quad (15)$$

$$\sigma_{P, \text{ann}} = \frac{1}{16\pi} \sum_f \left(\frac{G_{P,f}}{\sqrt{2}} \right)^2 c_f \sqrt{\frac{s - 4m_f^2}{s - 4M_\chi^2}} s \quad (16)$$

$$\sigma_{V, \text{ann}} = \frac{1}{12\pi} \sum_f \left(\frac{G_{V,f}}{\sqrt{2}} \right)^2 c_f \sqrt{\frac{s - 4m_f^2}{s - 4M_\chi^2}} \left[s + 2(M_\chi^2 + m_f^2) + 4 \frac{M_\chi^2 m_f^2}{s} \right] \quad (17)$$

$$\sigma_{A, \text{ann}} = \frac{1}{12\pi} \sum_f \left(\frac{G_{A,f}}{\sqrt{2}} \right)^2 c_f \sqrt{\frac{s - 4m_f^2}{s - 4M_\chi^2}} \left[s - 4(M_\chi^2 + m_f^2) + 28 \frac{M_\chi^2 m_f^2}{s} \right] \quad (18)$$

$$\sigma_{T, \text{ann}} = \frac{1}{6\pi} \sum_f \left(\frac{G_{T,f}}{\sqrt{2}} \right)^2 c_f \sqrt{\frac{s-4m_f^2}{s-4M_\chi^2}} \left[s + 2(M_\chi^2 + m_f^2) + 40 \frac{M_\chi^2 m_f^2}{s} \right] \quad (19)$$

$$\sigma_{SP, \text{ann}} = \frac{1}{16\pi} \sum_f \left(\frac{G_{SP,f}}{\sqrt{2}} \right)^2 c_f \sqrt{\frac{s-4m_f^2}{s-4M_\chi^2}} (s - 4M_\chi^2) \quad (20)$$

$$\sigma_{PS, \text{ann}} = \frac{1}{16\pi} \sum_f \left(\frac{G_{PS,f}}{\sqrt{2}} \right)^2 c_f \sqrt{\frac{s-4m_f^2}{s-4M_\chi^2}} (s - 4m_f^2) \quad (21)$$

$$\sigma_{VA, \text{ann}} = \frac{1}{12\pi} \sum_f \left(\frac{G_{VA,f}}{\sqrt{2}} \right)^2 c_f \sqrt{\frac{s-4m_f^2}{s-4M_\chi^2}} \left[s + 2(M_\chi^2 - 2m_f^2) - 8 \frac{M_\chi^2 m_f^2}{s} \right] \quad (22)$$

$$\sigma_{AV, \text{ann}} = \frac{1}{12\pi} \sum_f \left(\frac{G_{AV,f}}{\sqrt{2}} \right)^2 c_f \sqrt{\frac{s-4m_f^2}{s-4M_\chi^2}} \left[s + 2(m_f^2 - 2M_\chi^2) - 8 \frac{M_\chi^2 m_f^2}{s} \right] \quad (23)$$

$$\sigma_{\tilde{T}, \text{ann}} = \frac{2}{3\pi} \sum_f \left(\frac{\tilde{G}_{T,f}}{\sqrt{2}} \right)^2 c_f \sqrt{\frac{s-4m_f^2}{s-4M_\chi^2}} \left[s + 2(m_f^2 + M_\chi^2) - 32 \frac{M_\chi^2 m_f^2}{s} \right] \quad (24)$$

$$\begin{aligned} \sigma_{C, \text{ann}} &\equiv \sigma_{LL, \text{ann}} = \sigma_{RR, \text{ann}} = \sigma_{LR, \text{ann}} = \sigma_{RL, \text{ann}} \\ &= \frac{1}{3\pi} \sum_f \left(\frac{G_{C,f}}{\sqrt{2}} \right)^2 c_f \sqrt{\frac{s-4m_f^2}{s-4M_\chi^2}} \left[s - (M_\chi^2 + m_f^2) + 4 \frac{M_\chi^2 m_f^2}{s} \right] \end{aligned} \quad (25)$$

where s is the Mandelstam variable, M_χ is the WIMP mass, the sum is over the final state fermion species f , and c_f are the color factors, equal to 3 for quarks and 1 for leptons. The annihilation cross sections of the four chiral interactions, $\sigma_{LL, \text{ann}}$, $\sigma_{RR, \text{ann}}$, $\sigma_{LR, \text{ann}}$ and $\sigma_{RL, \text{ann}}$, have the exactly same formula, so they can be denoted by a common symbol $\sigma_{C, \text{ann}}$ with the corresponding coupling constants denoted by $G_{C,f}$. Note that Eqs.(15)–(17) agree exactly with Eqs.(6)–(8) in Ref. [32], while Eqs.(18),(19) are slightly different from Eqs.(9),(10) in [32].

In the very early Universe, the WIMPs were in thermal equilibrium. As the Universe expands, the WIMPs departed from thermal equilibrium when they were nonrelativistic, and finally froze out to yield a cold relic roughly when the annihilation rate dropped below the Hubble rate. This evolution process is described by the Boltzmann equation

$$\frac{dn_\chi}{dt} + 3Hn_\chi = -\langle \sigma_{\text{ann}} v_{\text{Mø}} \rangle [n_\chi n_{\bar{\chi}} - n_\chi^{\text{eq}} n_{\bar{\chi}}^{\text{eq}}] = -\langle \sigma_{\text{ann}} v_{\text{Mø}} \rangle [(n_\chi)^2 - (n_\chi^{\text{eq}})^2] \quad (26)$$

where $H \equiv \dot{a}/a = \sqrt{8\pi\rho/(3M_{\text{Pl}}^2)}$ is the Hubble rate with M_{Pl} denoting the Planck mass, n_χ ($n_{\bar{\chi}}$) is the number density of WIMPs (antiWIMPs), and the thermal average $\langle \sigma_{\text{ann}} v_{\text{Mø}} \rangle$ will be explained below. For Dirac fermions without particle-antiparticle asymmetry, $n_\chi = n_{\bar{\chi}}$, and the total DM particle number density is $n_{\text{DM}} = 2n_\chi$ [5, 48, 49]. At the early time, when the temperature $T \gg M_\chi$, the WIMP number density n_χ was very close to its equilibrium value $n_\chi^{\text{eq}} \propto T^3$, and the annihilation rate per unit volume $\Gamma = n_\chi n_{\bar{\chi}} \langle \sigma_{\text{ann}} v_{\text{Mø}} \rangle$ was much greater than the Hubble expansion rate per unit volume $3Hn_\chi$ and enough to maintain the thermal equilibrium. However, as the temperature T decreased below M_χ , the equilibrium number density was exponentially suppressed, $n_\chi^{\text{eq}} \simeq g[M_\chi T/(2\pi)]^{3/2} \exp(-M_\chi/T)$, where $g = 2$ is the number of degrees of freedom of a fermionic WIMP. Eventually, the annihilation rate became smaller than the expansion rate, and the WIMPs froze out of equilibrium.

The thermally averaged quantity $\langle \sigma_{\text{ann}} v_{\text{Mø}} \rangle$ should be treated carefully. As pointed out by Ref. [49], the Møller velocity $v_{\text{Mø}}$ in Eq. (26) is defined by $v_{\text{Mø}} \equiv \sqrt{(p_1 \cdot p_2)^2 - m_1^2 m_2^2} / (E_1 E_2) = \sqrt{|\mathbf{v}_1 - \mathbf{v}_2|^2 - |\mathbf{v}_1 \times \mathbf{v}_2|^2}$ with subscripts 1 and 2 labeling the two initial DM particles and particle velocities $\mathbf{v}_i \equiv \mathbf{p}_i/E_i$ ($i = 1, 2$). The Møller velocity $v_{\text{Mø}}$ equals the relative velocity $v_{\text{rel}} \equiv |\mathbf{v}_1 - \mathbf{v}_2|$ only when the collision is collinear, $\mathbf{v}_1 \times \mathbf{v}_2 = 0$. Since the Boltzmann equation, Eq. (26), is expressed in the cosmic comoving frame [49], in which the gas is at rest as a whole, the thermal average $\langle \sigma_{\text{ann}} v_{\text{Mø}} \rangle$ must be taken in this frame. Fortunately, even including relativistic effects, it has been shown [49] that $\langle \sigma_{\text{ann}} v_{\text{Mø}} \rangle = \langle \sigma_{\text{ann}} v_{\text{lab}} \rangle^{\text{lab}}$, where $v_{\text{lab}} \equiv |\mathbf{v}_{1, \text{lab}} - \mathbf{v}_{2, \text{lab}}|$ and the right-hand side is computed in the lab frame, in which one of the two initial particles is at rest. Thus, it is convenient to calculate the thermal average in the lab frame using the method described in [49].

Cold DM requires that the freeze-out of WIMPs occurred when they were nonrelativistic. In the nonrelativistic

limit, we can parameterize $\sigma_{\text{ann}}v = a + bv^2 + \mathcal{O}(v^4)$ ¹, where $v \equiv v_{\text{lab}} = \sqrt{s(s - 4M_\chi^2)/(s - 2M_\chi^2)}$. According to [48, 49], we then obtain $\langle \sigma_{\text{ann}}v \rangle^{\text{lab}} = a + 6b/x + \mathcal{O}(1/x^2)$ with $x \equiv M_\chi/T$. Now let us compute the coefficients a and b in the effective models. Due to the common factor $(s - 4M_\chi^2)^{-1/2}$ in Eqs. (15) – (25), s must be expanded up to order v^4 to get the correct coefficients b . In the lab frame, $s = 2M_\chi^2(1 + 1/\sqrt{1 - v^2}) = 4M_\chi^2 + M_\chi^2v^2 + \frac{3}{4}M_\chi^2v^4 + \mathcal{O}(v^6)$. Substituting this expansion of s into Eqs. (15) – (25) and expanding $\sigma_{\text{ann}}v$ in powers of v up to order v^2 , we obtain

$$\sigma_{S, \text{ann}}v \simeq \frac{1}{8\pi} \sum_f \left(\frac{G_{S,f}}{\sqrt{2}} \right)^2 c_f \left(1 - \frac{m_f^2}{M_\chi^2} \right)^{3/2} M_\chi^2 v^2 \quad (27)$$

$$\sigma_{P, \text{ann}}v \simeq \frac{1}{2\pi} \sum_f \left(\frac{G_{P,f}}{\sqrt{2}} \right)^2 c_f \sqrt{1 - \frac{m_f^2}{M_\chi^2}} M_\chi^2 \left[1 + \frac{m_f^2/M_\chi^2}{8(1 - m_f^2/M_\chi^2)} v^2 \right] \quad (28)$$

$$\sigma_{V, \text{ann}}v \simeq \frac{1}{2\pi} \sum_f \left(\frac{G_{V,f}}{\sqrt{2}} \right)^2 c_f \sqrt{1 - \frac{m_f^2}{M_\chi^2}} (2M_\chi^2 + m_f^2) \left[1 + \frac{-4 + 2m_f^2/M_\chi^2 + 11m_f^4/M_\chi^4}{24(1 - m_f^2/M_\chi^2)(2 + m_f^2/M_\chi^2)} v^2 \right] \quad (29)$$

$$\sigma_{A, \text{ann}}v \simeq \frac{1}{2\pi} \sum_f \left(\frac{G_{A,f}}{\sqrt{2}} \right)^2 c_f \sqrt{1 - \frac{m_f^2}{M_\chi^2}} m_f^2 \left[1 + \frac{8M_\chi^2/m_f^2 - 28 + 23m_f^2/M_\chi^2}{24(1 - m_f^2/M_\chi^2)} v^2 \right] \quad (30)$$

$$\sigma_{T, \text{ann}}v \simeq \frac{2}{\pi} \sum_f \left(\frac{G_{T,f}}{\sqrt{2}} \right)^2 c_f \sqrt{1 - \frac{m_f^2}{M_\chi^2}} (M_\chi^2 + 2m_f^2) \left[1 + \frac{-2 - 17m_f^2/M_\chi^2 + 28m_f^4/M_\chi^4}{24(1 - m_f^2/M_\chi^2)(1 + 2m_f^2/M_\chi^2)} v^2 \right] \quad (31)$$

$$\sigma_{SP, \text{ann}}v \simeq \frac{1}{8\pi} \sum_f \left(\frac{G_{SP,f}}{\sqrt{2}} \right)^2 c_f \sqrt{1 - \frac{m_f^2}{M_\chi^2}} M_\chi^2 v^2 \quad (32)$$

$$\sigma_{PS, \text{ann}}v \simeq \frac{1}{2\pi} \sum_f \left(\frac{G_{PS,f}}{\sqrt{2}} \right)^2 c_f \sqrt{1 - \frac{m_f^2}{M_\chi^2}} (M_\chi^2 - m_f^2) \left[1 + \frac{3m_f^2/M_\chi^2}{8(1 - m_f^2/M_\chi^2)} v^2 \right] \quad (33)$$

$$\sigma_{VA, \text{ann}}v \simeq \frac{1}{\pi} \sum_f \left(\frac{G_{VA,f}}{\sqrt{2}} \right)^2 c_f \sqrt{1 - \frac{m_f^2}{M_\chi^2}} (M_\chi^2 - m_f^2) \left[1 + \frac{-2 + 11m_f^2/M_\chi^2}{24(1 - m_f^2/M_\chi^2)} v^2 \right] \quad (34)$$

$$\sigma_{AV, \text{ann}}v \simeq \frac{1}{6\pi} \sum_f \left(\frac{G_{AV,f}}{\sqrt{2}} \right)^2 c_f \sqrt{1 - \frac{m_f^2}{M_\chi^2}} (M_\chi^2 + \frac{m_f^2}{2}) v^2 \quad (35)$$

$$\sigma_{\tilde{T}, \text{ann}}v \simeq \frac{8}{\pi} \sum_f \left(\frac{\tilde{G}_{T,f}}{\sqrt{2}} \right)^2 c_f \sqrt{1 - \frac{m_f^2}{M_\chi^2}} (M_\chi^2 - m_f^2) \left[1 + \frac{-2 + 17m_f^2/M_\chi^2}{24(1 - m_f^2/M_\chi^2)} v^2 \right] \quad (36)$$

$$\sigma_{C, \text{ann}}v \simeq \frac{2}{\pi} \sum_f \left(\frac{G_{C,f}}{\sqrt{2}} \right)^2 c_f \sqrt{1 - \frac{m_f^2}{M_\chi^2}} M_\chi^2 \left[1 + \frac{2 - m_f^2/M_\chi^2 + 2m_f^4/M_\chi^4}{24(1 - m_f^2/M_\chi^2)} v^2 \right] \quad (37)$$

from which, one can easily read off the corresponding thermally averaged quantities $\langle \sigma_{\text{ann}}v \rangle$. Our results of Eqs. (30), (35), and (37) agree well with Eqs. (35) and (39) of Ref. [48]. Note that Eq.(27) is the same as Eq.(13) in Ref. [32], while the $\mathcal{O}(v^2)$ terms of Eqs.(28)–(30), and both the $\mathcal{O}(v^0)$ and $\mathcal{O}(v^2)$ terms of Eq.(31) are different from the corresponding terms of Eq.(14)–(17) in [32]. In spite of these differences, they do not have much effect on the main results of Ref. [32]. This is because the calculated relic density depends mainly on the leading term of $\langle \sigma_{\text{ann}}v \rangle$, as we will see below.

Using the standard procedure [4, 5] to approximately solve the Boltzmann equation (26), we obtain a relic density of DM particles as

$$\Omega_{\text{DM}} h^2 = 2\Omega_\chi h^2 \simeq 2 \times 1.04 \times 10^9 \text{ GeV}^{-1} \left(\frac{T_0}{2.725 \text{ K}} \right)^3 \frac{x_f}{M_{\text{pl}} \sqrt{g_*(T_f)} (a + 3b/x_f)} \quad (38)$$

¹ Note that this expansion in powers of v_{lab}^2 is equivalent to that in Ref. [49]: $\sigma_{\text{ann}}v_{\text{lab}} = a^{(0)} + a^{(1)}\epsilon + \mathcal{O}(\epsilon^2)$ with $\epsilon \equiv (s - 4M_\chi^2)/(4M_\chi^2)$. Since $v_{\text{lab}} = 2\sqrt{\epsilon(1 + \epsilon)}/(1 + 2\epsilon)$, one easily obtains the relation between these two expansions: $a^{(0)} = a$, $a^{(1)} = 4b$, etc.

where $x_f \equiv M_\chi/T_f$ with T_f being the freeze-out temperature, $g_*(T_f)$ is the total number of effectively relativistic degrees of freedom at freeze-out, $T_0 = 2.725 \pm 0.002$ K [50] is the present CMB temperature. The freeze-out temperature parameter x_f can be evaluated by numerically solving the following equation:

$$x_f = \ln \left[c(c+2) \sqrt{\frac{45}{8}} \frac{g M_\chi M_{\text{Pl}} (a + 6b/x_f)}{2\pi^3 \sqrt{g_*(x_f)} x_f^{1/2}} \right] \quad (39)$$

where c is an order one parameter defined by the freeze-out criterion and determined by matching the late-time and early-time solutions. The precise value of c is not so significant for the numerical solution of x_f due to the logarithmic dependence in Eq. (39), and we take the usual value $c = 1/2$ in the calculation. Noting that g_* in Eqs. (38) and (39) depends on the temperature T , we adopt the recent numerical result of $g_*(T)$ in Ref. [51] where the quark-hadron transition temperature is taken to be 200 MeV.

According to the observed DM relic density, $\Omega_{\text{DM}} h^2 = 0.1109 \pm 0.0056$ [3], we can estimate the relation between the effective coupling constants G_f and the WIMP mass M_χ in each effective model of 4-fermion interaction operators, as shown in Fig. 1. Two kinds of coupling constants are considered here. In the upper frame of Fig. 1, we show the results for the case when the effective couplings to all the standard model fermions are equal (universal couplings). In the lower frame of Fig. 1, we show the results for the case when the coupling constants are proportional to the fermion mass m_f . In both cases, G_f decreases as M_χ increases for fixed $\Omega_{\text{DM}} h^2$ in each effective model. Besides, Fig. 1 has several interesting features:

- In both cases, the 4 curves of G_f vs. M_χ for the effective models of scalar, scalar-pseudoscalar, axialvector and axialvector-vector interactions lie well above the other curves. This comes from the fact that $\sigma_{S, \text{ann}v}$, $\sigma_{SP, \text{ann}v}$ and $\sigma_{AV, \text{ann}v}$ are of order $\mathcal{O}(v^2)$; although the leading term of $\sigma_{A, \text{ann}v}$ is of order $\mathcal{O}(v^0)$, it is smaller by a factor of m_f^2/M_χ^2 than the $\mathcal{O}(v^0)$ terms for other types of interactions.
- In the case of $G_f \propto m_f$, there is an obvious downward bend in the curve of G_f vs. M_χ at about $M_\chi \sim m_t = 171.2$ GeV in each effective model. This can be easily explained as follows. In the low velocity limit, the threshold for the annihilation channel $\chi \bar{\chi} \rightarrow t \bar{t}$ is about $M_\chi \sim m_t$. Since $G_f \propto m_f$, the WIMP couples much more strongly to the top quark than to other fermions, and the corresponding channel $\chi \bar{\chi} \rightarrow t \bar{t}$ gives a tremendous contribution to the total $\langle \sigma_{\text{ann}v} \rangle$. This finally makes the curve to bend down.
- In the case of universal couplings, there are 5 pairs of nearly identical curves, because in each pair their corresponding $\sigma_{\text{ann}v}$ differ only by terms of $\mathcal{O}(v^2)$ and/or terms of m_f^2/M_χ^2 . This feature is also noted in Ref. [32]. These pairs are: (1) the curves for scalar and scalar-pseudoscalar interactions, and we denote this approximate identity of the two curves by $S \simeq SP$ for short here and henceforth; (2) $P \simeq PS$; (3) $V \simeq VA$; (4) $T \simeq C$; (5) $A \simeq AV$ except for some small regions. From these approximate identities for pairs of curves, we see that the predicted relic density relies mainly on the leading term of $\langle \sigma_{\text{ann}v} \rangle$ in each model, especially on the $\mathcal{O}(M_\chi^2)$ term in the leading term.
- In the case of $G_f \propto m_f$, there are also 5 pairs of nearly identical curves except for some small regions. These pairs are the same as those in the above case, though deviations of the two nearly identical curves in each pair become large in this case.

In Fig. 2 we show the curves of $\Omega_{\text{DM}} h^2$ vs. M_χ for fixed coupling constants in the models of scalar, pseudoscalar, vector, axialvector, tensor and alternative tensor interaction operators. Due to the nearly identities described above, we do not include the curves for scalar-pseudoscalar, pseudoscalar-scalar, vector-axialvector, axialvector-vector and chiral interactions. Here we still consider the two kinds of coupling constants. In the upper left and upper right frames, we show the results when the coupling constants are proportional to the standard model fermion masses, $G_f \propto m_f$, and various values of the couplings are taken: $G_f \times (1 \text{ GeV}/m_f) = 10^{-8}, 10^{-7}, 10^{-6}, 10^{-5}$ and 10^{-4} GeV^{-2} . This proportionality of the couplings to the fermion masses may come from Yukawa couplings of a Higgs mediated interaction or some other unknown underlying mechanism. In the remaining 6 frames, we show the results for the case when the effective couplings to all the standard model fermions are equal (universal couplings), and various values of the couplings are taken: $G_f = 10^{-8}, 10^{-7}, 10^{-6}, 10^{-5}$ and 10^{-4} GeV^{-2} . The curves in Fig. 2 bend down to more or less at about $M_\chi \sim 1.72$ GeV, 4.20 GeV and 171.2 GeV, which exactly correspond to the masses of charm, bottom, top quarks, respectively.

Comparing with the results in Ref. [32], we observe that the curves in the first 6 frames of Fig. 2 are a little higher than those given by Ref. [32]. This slight difference may be caused by the following reasons: (1) We use $\Omega_{\text{DM}} = \Omega_\chi + \Omega_{\bar{\chi}} = 2\Omega_\chi$ for Dirac fermionic WIMPs with the assumption of no particle-antiparticle asymmetry. (2) Some formulas of $\sigma_{\text{ann}v}$ we obtained differ slightly from those given by [32], as already described at the bottom of Eq.(37). (3) We use the effective degrees of freedom $g_*(T)$ given by [51].

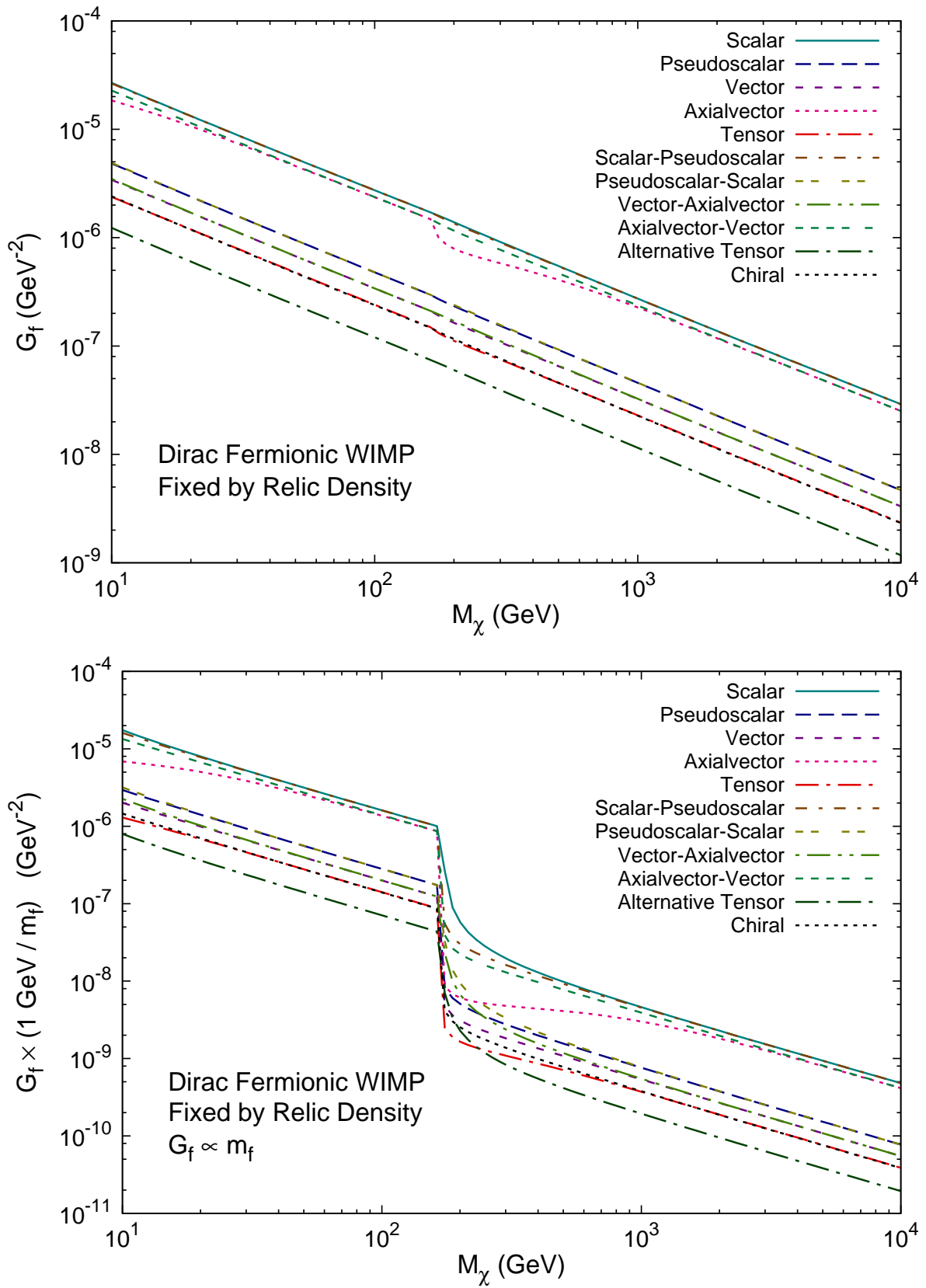


FIG. 1. The predicted coupling constant G_f as a function of the WIMP mass M_χ , fixed by the observed relic density, $\Omega_{\text{DM}} h^2 = 0.1109 \pm 0.0056$ [3], in each effective model of 4-fermion interaction operators. In the upper frame, results are given for the case when the effective couplings to all the standard model fermions are equal (universal couplings). In the lower frame, results are shown for the case when the coupling constants are proportional to the fermion mass m_f . In both cases, several pairs of curves are nearly identical. See the text for more details.

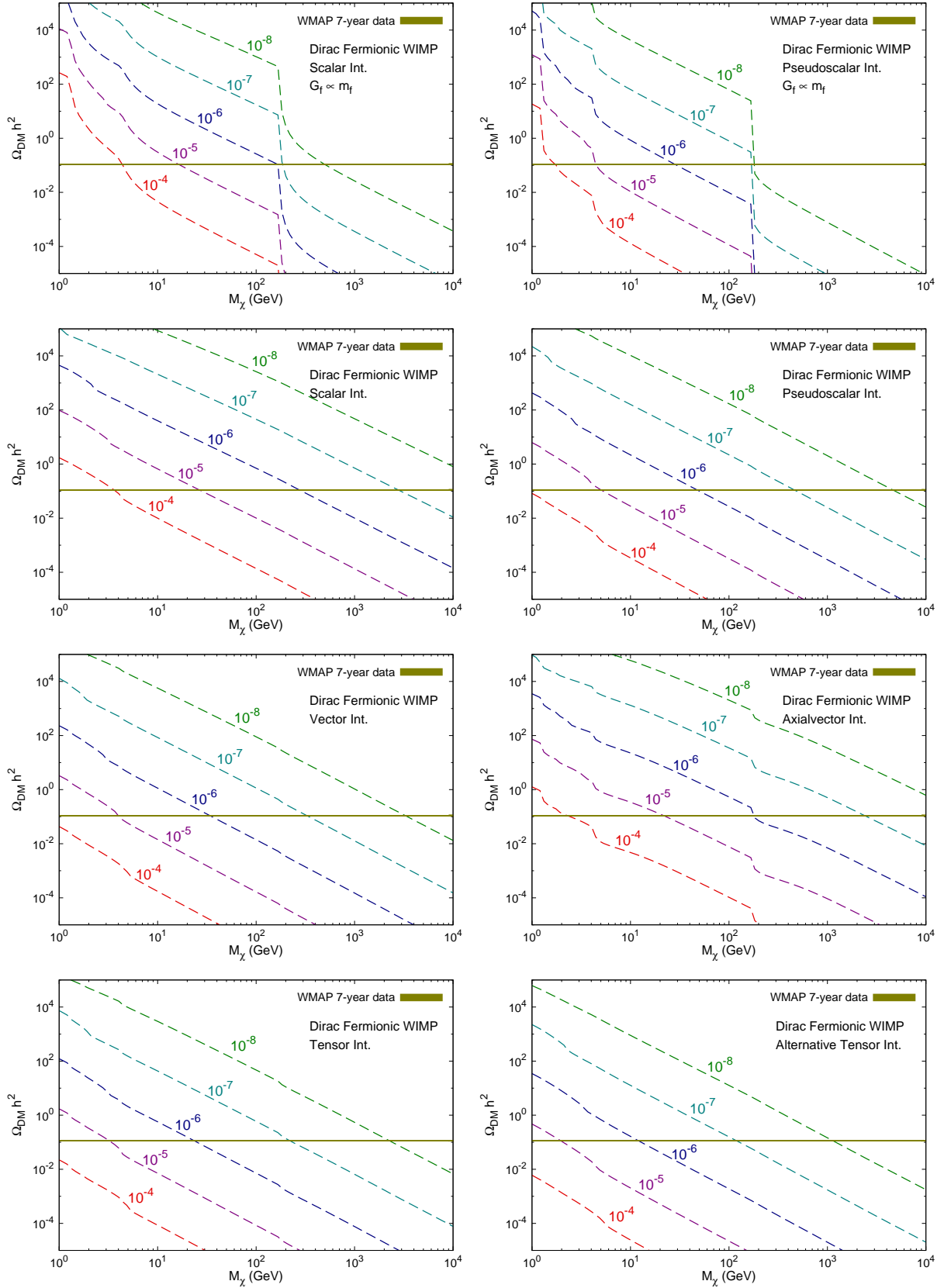


FIG. 2. The predicted thermal relic density (dashed lines) of Dirac fermionic WIMPs with scalar, pseudoscalar, vector, axialvector, tensor and alternative tensor interactions respectively. In the upper left and upper right frames, results are given for the case when the coupling constants are proportional to the fermion mass m_f , $G_f \times (1 \text{ GeV}/m_f) = 10^{-8}, 10^{-7}, 10^{-6}, 10^{-5}$ and 10^{-4} GeV^{-2} . In the remaining 6 frames, results are shown for the case when the couplings to all the standard model fermions are equal (universal couplings), $G_f = 10^{-8}, 10^{-7}, 10^{-6}, 10^{-5}$ and 10^{-4} GeV^{-2} . The horizontal solid band shows the range of the observed DM relic density, $\Omega_{\text{DM}} h^2 = 0.1109 \pm 0.0056$, measured by WMAP [3].

It is important to note that the results in Figs. 1 and 2 are found under the assumptions presented in Sec. II. If resonances, coannihilations, or annihilations to final states other than fermion-antifermion pairs are significant, the actual curves in Figs. 1 and 2 will be significantly lower than these shown there, as pointed out in [32].

IV. DIRECT DETECTION

In this section we discuss the direct detection constraints on the effective models of Eqs.(1)–(14). Direct detection experiments are designed to measure the recoil energy of the atomic nuclei when the WIMPs elastically scatter off them. The WIMP-quark interactions in the effective models naturally induce the WIMP-nucleon interactions, and the latter further induce the WIMP-nucleus interactions. Such interactions may lead to the elastic scattering of the WIMPs with the nuclei, which may be detected at the direct detection experiments.

The velocity of the WIMP near the Earth is thought to be of the same order as the orbital velocity of the Sun, $v \simeq 0.001c$. Because of this small velocity, the momentum transfer in the WIMP-nucleus scattering is considerably small compared to the masses of the WIMP and the nuclei. Thus all the WIMP-nucleus cross sections can be calculated in the limit of zero momentum transfer. In this limit the WIMP-quark interaction operators, \mathcal{L}_P , \mathcal{L}_{SP} , \mathcal{L}_{PS} , \mathcal{L}_{VA} , \mathcal{L}_{AV} and $\mathcal{L}_{\bar{T}}$, and their correspondingly induced WIMP-nucleon interaction operators have no contribution to the WIMP-nucleus cross sections and thus they are not sensitive to direct detection experiments. This is because in the zero momentum transfer limit some fermion bilinear operators become zero, for example, the operator $\bar{\psi}\gamma_5\psi$ vanishes, and the time component of $\bar{\psi}\gamma^\mu\gamma_5\psi$ and the space components of $\bar{\psi}\gamma^\mu\psi$ vanish as well. For more details on this issue, see Ref. [52].

Among the remaining operators relevant to direct detection, the scalar and vector interaction operators, \mathcal{L}_S and \mathcal{L}_V , are referred to as spin-independent (SI) interactions, while the axialvector and tensor interaction, \mathcal{L}_A and \mathcal{L}_T , belong to spin-dependent (SD) interactions. And the chiral interaction operators are the combinations of SI and SD interactions. The SI interactions of all the nucleons add coherently in the target nucleus, and the corresponding WIMP-nucleus cross section is proportional to the square of the atomic mass number of the nucleus. On the other hand, since the spins of nucleons in a nucleus tend to cancel in pairs, the SD interactions rely mainly on the spin content of one unpaired nucleon and the corresponding cross section is not enhanced for heavy nuclei.

We would like to illustrate the calculation in the effective model of scalar interaction operators. Eq.(1) can induce the effective Lagrangian for the WIMP-nucleon couplings, which reads

$$\mathcal{L}_{S, \text{induced}} = \sum_{N=p,n} \frac{G_{S,N}}{\sqrt{2}} \bar{\chi}\chi \bar{N}N \quad (40)$$

where the WIMP's effective Fermi couplings to the nucleons (protons and neutrons), $G_{S,N}$ ($N = p, n$), are related to the coupling constants to quarks by

$$G_{S,N} = \sum_{q=u,d,s} G_{S,q} f_q^N \frac{m_N}{m_q} + \sum_{q=c,b,t} G_{S,q} f_Q^N \frac{m_N}{m_q} \quad (41)$$

where the nucleon form factors are $f_u^p = 0.020 \pm 0.004$, $f_d^p = 0.026 \pm 0.005$, $f_s^p = 0.118 \pm 0.062$, $f_u^n = 0.014 \pm 0.003$, $f_d^n = 0.036 \pm 0.008$, $f_s^n = 0.118 \pm 0.062$ [53], and

$$f_Q^N = \frac{2}{27} \left(1 - \sum_{q=u,d,s} f_q^N \right) \quad (42)$$

From Eq.(40) and its induced WIMP-nucleus interactions, it follows that the cross section for a WIMP (χ) scattering elastically from a nucleus (A) in the zero momentum transfer limit is given by [54]

$$\text{Scalar Int. :} \quad \sigma_{S, \chi A} = \frac{4}{\pi} \frac{M_\chi^2 m_A^2}{(M_\chi + m_A)^2} \left[\frac{1}{2} \left(Z \frac{G_{S,p}}{\sqrt{2}} + (A - Z) \frac{G_{S,n}}{\sqrt{2}} \right) \right]^2 \quad (43)$$

where m_A is the target nucleus mass. Z and $(A - Z)$ are the numbers of protons and neutrons in the nucleus. The factor $1/2$ in the square bracket comes from the fact that a Dirac fermionic WIMP and its antiparticle are different [54]. However, this factor is missing in Eq.(20) of Ref.[32]. Indeed, such a factor $1/2$ does not exist in the expression for a self-conjugated WIMP such as a Majorana fermion, but it seems that a Dirac fermionic WIMP is considered in Ref.[32], otherwise the fermion bilinears $\bar{\chi}\gamma^\mu\chi$ and $\bar{\chi}\sigma^{\mu\nu}\chi$ vanish for a Majorana fermion χ . Taking the special case

when the nucleus is just the nucleon (proton or neutron) in Eq.(43), we obtain the WIMP-nucleon cross section in the zero momentum transfer limit:

$$\text{Scalar Int. : } \quad \sigma_{S, \chi N} = \frac{M_\chi^2 m_N^2}{\pi(M_\chi + m_N)^2} \left(\frac{G_{S,N}}{\sqrt{2}} \right)^2 \quad (44)$$

Likewise, we compute the WIMP-nucleus cross section in the effective models of vector, axialvector, tensor and chiral interaction operators, resulting in

$$\text{Vector Int. : } \quad \sigma_{V, \chi A} = \frac{M_\chi^2 m_A^2}{\pi(M_\chi + m_A)^2} \left[Z \frac{G_{V,p}}{\sqrt{2}} + (A - Z) \frac{G_{V,n}}{\sqrt{2}} \right]^2 \quad (45)$$

$$\text{Axialvector Int. : } \quad \sigma_{A, \chi A} = \frac{4M_\chi^2 m_A^2}{\pi(M_\chi + m_A)^2} \frac{J_A + 1}{J_A} \left[\frac{G_{A,p}}{\sqrt{2}} S_p^A + \frac{G_{A,n}}{\sqrt{2}} S_n^A \right]^2 \quad (46)$$

$$\text{Tensor Int. : } \quad \sigma_{T, \chi A} = \frac{16M_\chi^2 m_A^2}{\pi(M_\chi + m_A)^2} \frac{J_A + 1}{J_A} \left[\frac{G_{T,p}}{\sqrt{2}} S_p^A + \frac{G_{T,n}}{\sqrt{2}} S_n^A \right]^2 \quad (47)$$

$$\begin{aligned} \text{Chiral Int. : } \quad \sigma_{C, \chi A} &= \frac{M_\chi^2 m_A^2}{\pi(M_\chi + m_A)^2} \left[Z \frac{G_{V,p}}{\sqrt{2}} + (A - Z) \frac{G_{V,n}}{\sqrt{2}} \right]^2 \\ &\quad + \frac{4M_\chi^2 m_A^2}{\pi(M_\chi + m_A)^2} \frac{J_A + 1}{J_A} \left[\frac{G_{A,p}}{\sqrt{2}} S_p^A + \frac{G_{A,n}}{\sqrt{2}} S_n^A \right]^2 \\ &\simeq \frac{M_\chi^2 m_A^2}{\pi(M_\chi + m_A)^2} \left[Z \frac{G_{V,p}}{\sqrt{2}} + (A - Z) \frac{G_{V,n}}{\sqrt{2}} \right]^2 \quad (\text{when } A \gg 1) \end{aligned} \quad (48)$$

where J_A is the nuclear spin, S_N^A is the expectation value of the total spin of the nucleon (N) in the nucleus (A), and the WIMP's effective Fermi couplings, G_N , to the nucleons are related to those to quarks, G_q , by

$$G_{V,p} = 2G_{V,u} + G_{V,d}, \quad G_{V,n} = G_{V,u} + 2G_{V,d} \quad (49)$$

$$G_{A,N} = \sum_{q=u,d,s} G_{A,q} \Delta_q^N \quad (50)$$

$$G_{T,N} = \sum_{q=u,d,s} G_{T,q} \Delta_q^N \quad (51)$$

with the form factors $\Delta_u^p = 0.842 \pm 0.012$, $\Delta_d^p = -0.427 \pm 0.013$, $\Delta_s^p = -0.085 \pm 0.018$ [55], $\Delta_u^n = \Delta_d^p$, $\Delta_d^n = \Delta_u^p$, $\Delta_s^n = \Delta_s^p$. In Eq.(48) the WIMP-nucleus cross section for chiral interactions receives contributions from both SI and SD interactions. As heavy nuclei are used in CDMS and XENON, the SD part in Eq.(48) is several orders of magnitude smaller than the SI part, and thus the SD contribution may be omitted when comparing the results in those experiments. So, in this approximation, the WIMP-nucleus cross section for chiral interactions has the same form as that for vector interactions. The WIMP-nucleus cross sections in Eqs. (45) – (48) can be normalized to the corresponding WIMP-nucleon cross sections as follows:

$$\text{Vector Int. : } \quad \sigma_{V, \chi N} = \frac{M_\chi^2 m_N^2}{\pi(M_\chi + m_N)^2} \left(\frac{G_{V,N}}{\sqrt{2}} \right)^2 \quad (52)$$

$$\text{Axialvector Int. : } \quad \sigma_{A, \chi N} = \frac{3M_\chi^2 m_N^2}{\pi(M_\chi + m_N)^2} \left(\frac{G_{A,N}}{\sqrt{2}} \right)^2 \quad (53)$$

$$\text{Tensor Int. : } \quad \sigma_{T, \chi N} = \frac{12M_\chi^2 m_N^2}{\pi(M_\chi + m_N)^2} \left(\frac{G_{T,N}}{\sqrt{2}} \right)^2 \quad (54)$$

$$\text{Chiral Int. : } \quad \tilde{\sigma}_{C, \chi N} \simeq \frac{M_\chi^2 m_N^2}{\pi(M_\chi + m_N)^2} \left(\frac{G_{V,N}}{\sqrt{2}} \right)^2 \quad (55)$$

Note that in Eq.(55) $\tilde{\sigma}_{C, \chi N}$ is not the actual WIMP-nucleon cross section for chiral interactions, it just means a normalized quantity of the corresponding WIMP-nucleus cross section for a heavy nucleus A . In other words, a normalization procedure from Eq.(48) to Eq.(55) is used: $\tilde{\sigma}_{C, \chi N} \equiv [\mu_N^2 / (\mu_A^2 A^2)] \cdot \sigma_{C, \chi A}$ when $A \gg 1$, with the reduced masses $\mu_A \equiv M_\chi m_A / (M_\chi + m_A)$ and $\mu_N \equiv M_\chi m_N / (M_\chi + m_N)$, where we have used the fact that $G_{V,p}$ and $G_{V,n}$ have the same order of magnitude: $G_{V,p} \sim G_{V,n}$.

Eqs. (44), (52) – (55) predict the normalized WIMP-nucleon cross sections $\sigma_{\chi N}$ for the different interactions as functions of the WIMP mass M_χ and the effective couplings to nucleons G_N , which further depend on the more

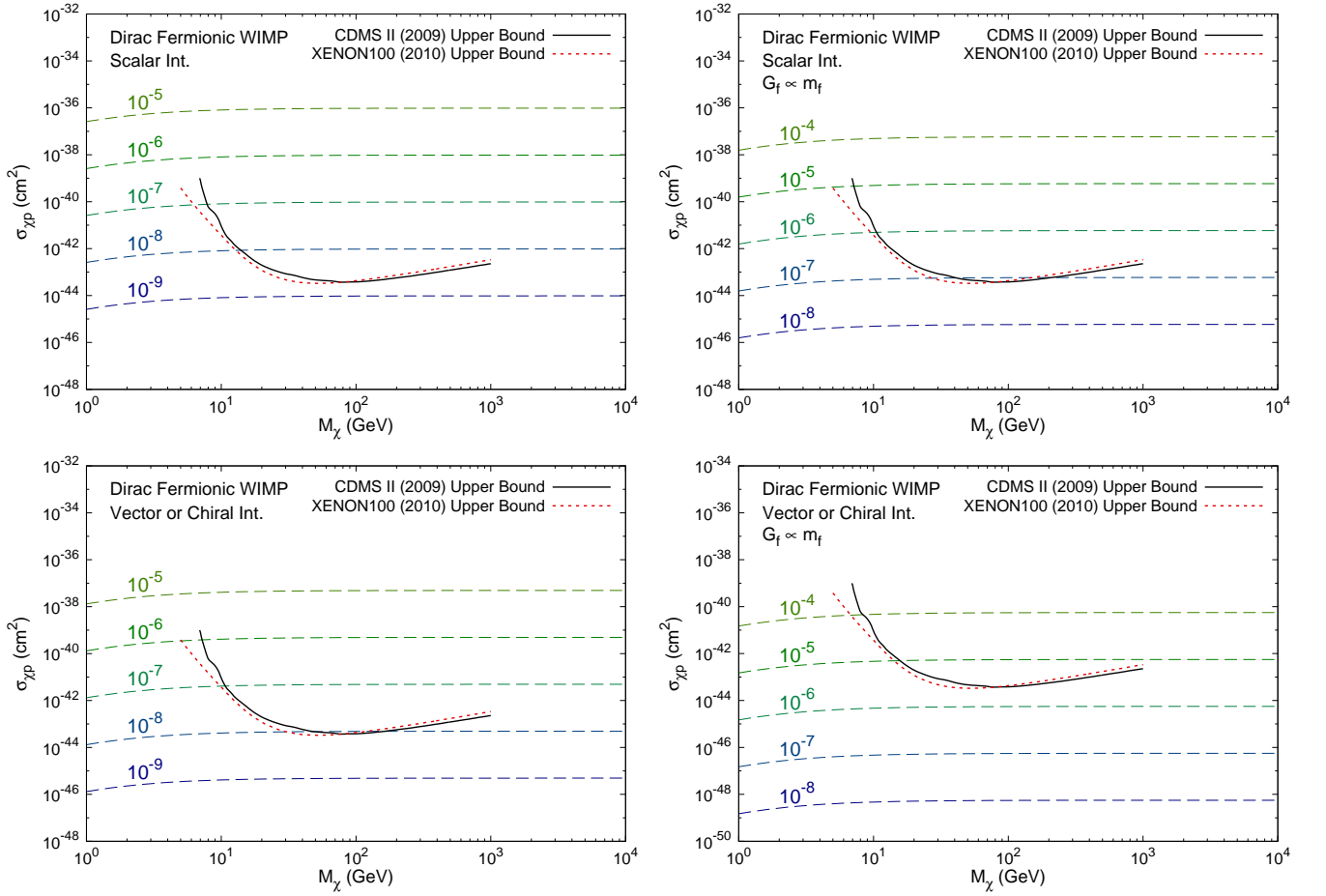


FIG. 3. The spin-independent (SI) WIMP-proton cross sections (dashed lines) for Dirac fermionic WIMPs with scalar, vector and chiral interactions. The results for chiral interactions are approximately identical to those for vector interactions. In the upper left and lower left frames, the results are shown for scalar and vector interactions for the case of universal couplings $G_f = 10^{-9}, 10^{-8}, 10^{-7}, 10^{-6}$ and 10^{-5} GeV^{-2} . In the remaining two frames, the results are shown for the case when the coupling constants proportion to the fermion mass m_f , $G_f \times (1 \text{ GeV}/m_f) = 10^{-8}, 10^{-7}, 10^{-6}, 10^{-5}$ and 10^{-4} GeV^{-2} . Also shown as solid and dotted curves are the current upper bounds from the experiments of CDMS II (2009) [44] and XENON100 (2010) [45].

fundamental effective couplings to quarks G_q . To illustrate the results and compare with the experimental bounds, we draw the curves of $\sigma_{\chi N}$ vs. M_χ for fixed coupling constants in these effective models.

In Fig. 3, we show the SI cross sections for a Dirac WIMP elastically scattering with a proton in the effective models of scalar, vector and chiral interactions, respectively. The results for chiral interactions are approximately identical to those for vector interactions due to Eqs. (52) and (55), so they are shown in the same frame. We still consider the two types of coupling constants. In the upper left and lower left frames of Fig. 3, the results are shown for scalar and vector interactions for the case of universal couplings $G_f = 10^{-9}, 10^{-8}, 10^{-7}, 10^{-6}$ and 10^{-5} GeV^{-2} . In the remaining two frames, the results are shown for the case when the coupling constants proportional to the fermion mass m_f , $G_f \times (1 \text{ GeV}/m_f) = 10^{-8}, 10^{-7}, 10^{-6}, 10^{-5}$ and 10^{-4} GeV^{-2} . We also show in Fig. 3 the current upper limits for the SI WIMP-nucleon elastic scattering from the experiments of CDMS II (2009) [44] and XENON100 (2010) [45] for comparison.

In Fig. 4, we show the SD cross sections for a Dirac WIMP elastically scattering with a neutron in the effective models of axialvector and tensor interactions, respectively. In the upper left and lower left frames of Fig. 4, the results are shown for axialvector and tensor interactions for the case of universal couplings $G_f = 10^{-6}, 10^{-5}, 10^{-4}, 10^{-3}$ and 10^{-2} GeV^{-2} . In the remaining two frames, the results are shown for the case when the coupling constants proportional to the fermion mass m_f , $G_f \times (1 \text{ GeV}/m_f) = 10^{-4}, 10^{-3}, 10^{-2}, 10^{-1}$ and 1 GeV^{-2} . Also shown in Fig. 4 are the upper bounds for the SD WIMP-neutron elastic scattering from the experiments of CDMS (2005) [46] and XENON10 (2008) [47].

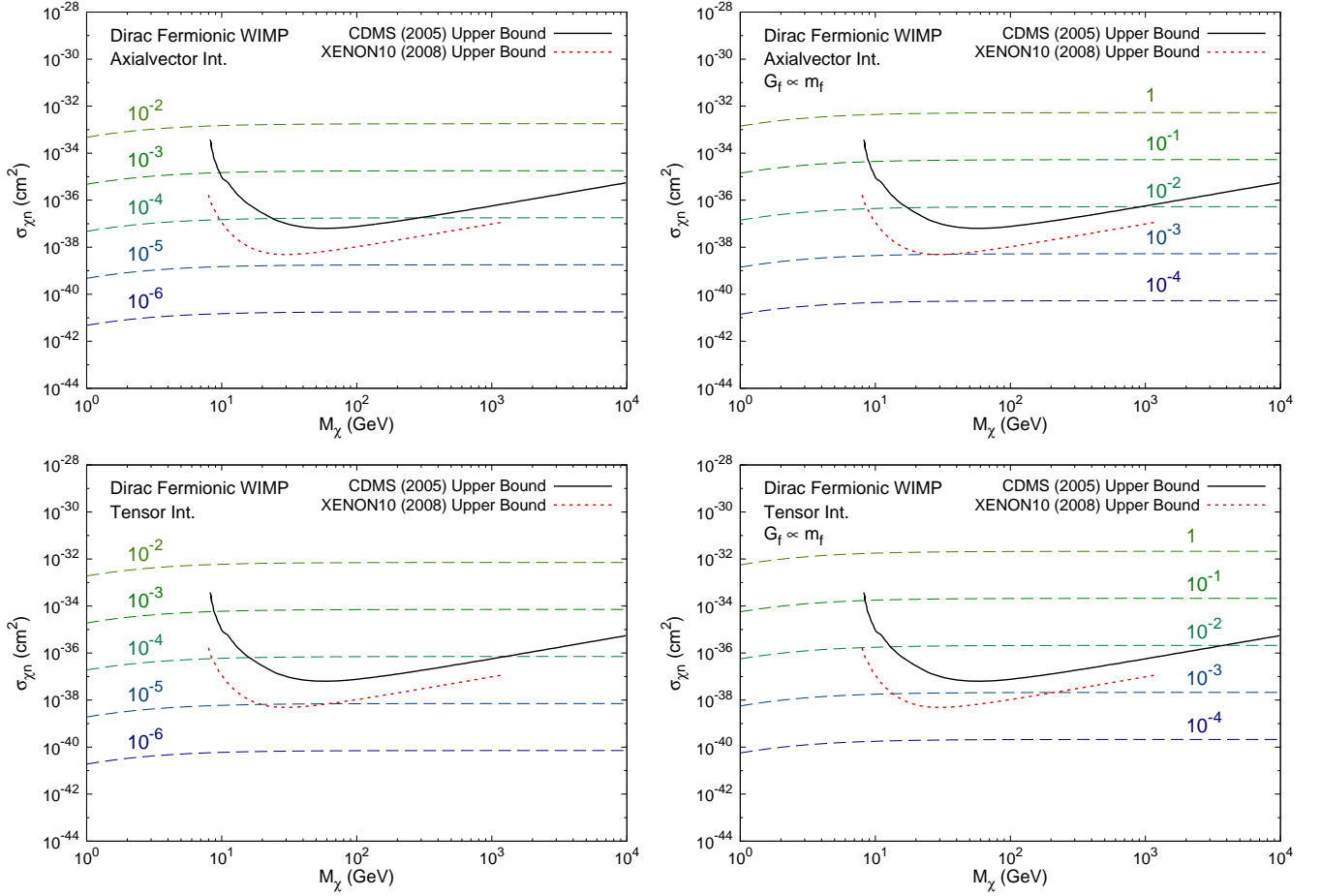


FIG. 4. The spin-dependent (SD) WIMP-neutron cross sections (dashed lines) for Dirac fermionic WIMPs with axialvector and tensor interactions. In the upper left and lower left frames, the results are shown for axialvector and tensor interactions for the case of universal couplings $G_f = 10^{-6}, 10^{-5}, 10^{-4}, 10^{-3}$ and 10^{-2} GeV^{-2} . In the remaining two frames, the results are shown for the case when the coupling constants proportion to the fermion mass m_f , $G_f \times (1 \text{ GeV}/m_f) = 10^{-4}, 10^{-3}, 10^{-2}, 10^{-1}$ and 1 GeV^{-2} . Also shown as solid and dotted curves are the upper bounds from the experiments of CDMS (2005) [46] and XENON10 (2008) [47].

From Figs. 3 and 4, we see that the experimental constraints for the SI interactions (i.e., scalar or vector interactions) are much more stringent than those for the SD interactions (i.e., axialvector or tensor interactions). In addition, the experimental constraints in the case of universal couplings are more stringent than those in the case of Yukawa-like couplings ($G_f \propto m_f$) for both the SI and SD interactions. Due to the factor 4 difference in the WIMP-nucleon cross sections between us and that in [32] our predicted WIMP-proton SI cross sections (dashed lines) in Figs. 3 are lower than them.

We summarize that the scalar, vector and chiral interactions are mainly constrained by the experimental SI upper limits of WIMP-nucleus elastic scattering, while the axialvector and tensor interactions are constrained by the SD upper limits of WIMP-nucleus elastic scattering. However, the other 6 types of interactions, \mathcal{L}_P , \mathcal{L}_{SP} , \mathcal{L}_{PS} , \mathcal{L}_{VA} , \mathcal{L}_{AV} and $\mathcal{L}_{\bar{T}}$, cannot be constrained by direct detection experiments.

V. INDIRECT DETECTION

In addition to the direct search method for the WIMP DM at underground laboratories, an indirect detection method is used to look for the DM annihilation or decay products which include neutrinos, gamma rays, positrons and antiprotons. These particles can be detected by cosmic ray experiments. For the charged particles they are deflected by the Galactic magnetic field and interact with the interstellar medium when they propagate in the Galaxy. Therefore we have to study the propagation process of the charged particles to compare predictions with observations.

The propagation of cosmic rays in the Galaxy can be described by [56]

$$\frac{\partial \psi}{\partial t} = Q(\vec{r}, p) + \nabla \cdot (D_{xx} \nabla \psi - \vec{V}_c \psi) + \frac{\partial}{\partial p} \left[p^2 D_{pp} \frac{\partial}{\partial p} \left(\frac{1}{p^2} \psi \right) \right] - \frac{\partial}{\partial p} \left[\dot{p} \psi - \frac{p}{3} (\nabla \cdot \vec{V}_c) \psi \right] - \frac{1}{\tau_f} \psi - \frac{1}{\tau_r} \psi \quad (56)$$

where $\psi = \psi(\vec{r}, p, t)$ is the number density of cosmic-ray particles per unit momentum interval, $Q(\vec{r}, p)$ is the source term, D_{xx} is the spatial diffusion coefficient, \vec{V}_c is the convection velocity, D_{pp} is the diffusion coefficient in momentum space describing the reacceleration process, $\dot{p} \equiv dp/dt$ is the momentum loss rate, τ_f and τ_r are the time scales for fragmentation and the radioactive decay, respectively. The most accurate method to treat the propagation is to solve Eq. (56) by a numerical code, GALPROP [56, 57]. For given source functions and boundary conditions, GALPROP can solve the equations for various cosmic-ray species and give reasonable fit to many cosmic ray data.

Antiprotons are rarely produced in usual astrophysical processes, and the observed antiproton-to-proton flux ratio \bar{p}/p is small, typically $\mathcal{O}(10^{-5}) \sim \mathcal{O}(10^{-4})$, from 100 MeV to 100 GeV in kinetic energy. The annihilation of WIMPs, however, produces protons and antiprotons in equal numbers. Thus the \bar{p}/p spectrum may be sensitive to the annihilation of WIMPs. In this work we use the antiproton-to-proton flux ratio \bar{p}/p measured by the satellite-borne experiment PAMELA [58] to constrain the effective models.

The source term of antiprotons contributed by the annihilation of Dirac fermionic WIMPs is given by

$$Q_{\text{ann}}(\mathbf{x}, E) = \frac{\langle \sigma_{\text{ann}} v \rangle_{\text{tot}}}{4M_\chi^2} \left[\sum_q B_q \left(\frac{dN_{\bar{p}}}{dE_{\bar{p}}} \right)_q \right] \rho^2(\mathbf{x}), \quad (57)$$

with

$$\langle \sigma_{\text{ann}} v \rangle_{\text{tot}} = \sum_q \langle \sigma_{\text{ann}} v \rangle_q, \quad \text{and} \quad B_q = \frac{\langle \sigma_{\text{ann}} v \rangle_q}{\langle \sigma_{\text{ann}} v \rangle_{\text{tot}}}, \quad q = u, d, s, c, b, t, \quad (58)$$

where $\rho(\mathbf{x})$ is the DM mass density distribution of the Galaxy, $(dN_{\bar{p}}/dE_{\bar{p}})_q$ is the number per unit energy interval of the antiprotons produced by the annihilation of a pair of WIMPs in the $q\bar{q}$ channel, and B_q is the branching ratio of the $q\bar{q}$ channel. The source term of protons is similar to Eq.(57). We use the Monte Carlo program PYTHIA [59] to simulate the particle production of the WIMP annihilation processes, and pick out the events in which the final states are \bar{p} to build the $(dN_{\bar{p}}/dE_{\bar{p}})_q$ spectrum in each quark-antiquark channel. Due to the different quark masses, the $(dN_{\bar{p}}/dE_{\bar{p}})_q$ spectra in the six $q\bar{q}$ channels are slightly different.

The NFW profile [60] is taken to describe the DM mass density distribution of the Galaxy:

$$\rho(r) = \frac{\rho_s}{(r/r_s)(1+r/r_s)^2}, \quad (59)$$

where ρ_s is the characteristic density, and r_s is the scale radius. We choose $\rho_s = 0.334 \text{ GeV/cm}^3$ and $r_s = 20 \text{ kpc}$. These values guarantee the local DM density $\rho(8.33 \text{ kpc}) = 0.4 \text{ GeV/cm}^3$, which is consistent with the recent results, such as [61] and [62]. The CDM particles in the Galaxy should obey the Maxwell-Boltzmann velocity distribution $f(v_0) = (M_\chi/2\pi k_B T)^{3/2} \exp(-M_\chi v_0^2/2k_B T)$. Their velocity dispersion $\bar{v} \equiv \sqrt{\langle v_0^2 \rangle}$ is chosen to be the canonical value 270 km/s [5]. Since the DM particles in the Galaxy nowadays are extremely nonrelativistic, v_{Mol} almost equals v_{rel} by neglecting the $\mathcal{O}(v^2/c^2)$ term, and we need not to distinguish them. And v_{rel} has the same value in different frames with the extremely nonrelativistic limit. Thus, as a very good approximation, we expand $\langle \sigma_{\text{ann}} v \rangle$ to be $\langle \sigma_{\text{ann}} v \rangle \simeq a + b \langle v^2 \rangle$ with the coefficients a and b obtained in Eqs. (27)–(37). The relation between $\langle v^2 \rangle$ and \bar{v} is given by $\langle v^2 \rangle = \langle \mathbf{v}_1^2 - 2\mathbf{v}_1 \cdot \mathbf{v}_2 + \mathbf{v}_2^2 \rangle = 2 \langle v_0^2 \rangle = 2\bar{v}^2$.

In the calculation of the \bar{p}/p spectrum with GALPROP, we adopt the Galaxy propagation model with diffusion and convection, and set the half-height of the Galaxy propagation halo to be $z_h = 4 \text{ kpc}$. Although the GALPROP expected \bar{p}/p spectrum without the DM contribution can fit the PAMELA result [58] well, as shown in the left frame of Fig. 5, the present data cannot rule out the possibility that the \bar{p}/p spectrum might receive a small portion of contribution from the DM annihilation. If we add the DM contribution to the \bar{p}/p spectrum, however, the total spectrum (GALPROP background + DM contribution) may deviate from the PAMELA result, as shown in the right frame of Fig. 5. For the universal couplings and the Yukawa-like couplings ($G_f \propto m_f$) in our numerical calculation, the DM contribution is actually determined by two parameters, $\langle \sigma_{\text{ann}} v \rangle_{\text{tot}}$ and M_χ . For fixed M_χ , the smaller $\langle \sigma_{\text{ann}} v \rangle_{\text{tot}}$ is, the smaller the DM contribution will be. We must let $\langle \sigma_{\text{ann}} v \rangle_{\text{tot}}$ be small enough to keep the total \bar{p}/p spectrum within an acceptable deviation range of the PAMELA result when we take into account the DM contribution.

Now we calculate the χ^2 value to set upper bound on the DM coupling constants from the \bar{p}/p data. Since $\langle \sigma_{\text{ann}} v \rangle_{\text{tot}}$ monotonously depends on the coupling constants G_f , we can derive the 3σ upper bounds on G_f for fixed M_χ in the

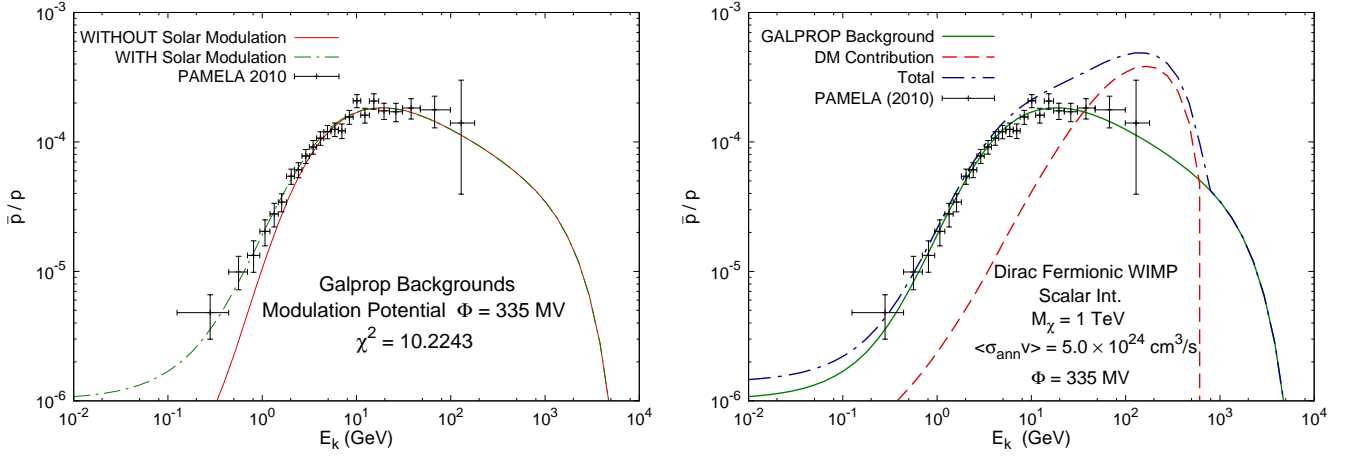


FIG. 5. The \bar{p}/p spectrum calculated by GALPROP and that measured by PAMELA [58] (error bars). In the left frame, we show the GALPROP predicted \bar{p}/p spectrum without the DM contribution, where the Solar modulation potential Φ is taken to be 335 MV to fit the PAMELA data. In the right frame, we show the predicted total \bar{p}/p spectrum (GALPROP background + DM contribution) in the effective model of scalar interactions as an example. $M_\chi = 1$ TeV and $\langle \sigma_{\text{ann}} v \rangle_{\text{tot}} = 5.0 \times 10^{24}$ cm³/s are set here.

cases of universal couplings and Yukawa-like couplings ($G_f \propto m_f$) for each type of effective interactions, as shown in Fig. 6. Here the solar modulation potential is set to be $\Phi = 335$ MV, which gives minimal χ^2 for the background only.

We see that several pairs of upper bound curves in Fig. 6 are nearly identical, which is similar to the situation of Fig. 1. The reason is the same as explain before. As pointed out in Sec. III, the quantity $\sigma_{\text{ann}} v$ in each pair differ only by terms of $\mathcal{O}(v^2)$ and/or terms of m_f^2/M_χ^2 . Using the abbreviated notation defined in Sec. III, we may call the pairs of nearly identical upper bound curves by $S \simeq SP$, $P \simeq PS$, $V \simeq VA$, and $T \simeq C$. These 4 pairs are the same as those in Fig. 1 in Sec. III. The exception in this situation is that the upper bound curves for axialvector (A) and axialvector-vector (AV) interactions are rather different. It may comes from the fact that $\sigma_{AV, \text{ann}} v$ is of order $\mathcal{O}(v^2)$, while $\sigma_{A, \text{ann}} v$ is of order $\mathcal{O}(v^0)$ and proportional to m_f^2 . The difference of the curves for A and AV is somewhat like the difference of the cases of universal couplings and Yukawa-like couplings ($G_f \propto m_f$) for the same effective interaction. In addition, we note that in Fig. 6 the upper bound curves for scalar (S), scalar-pseudoscalar (SP) and axialvector-vector (AV) interactions lie well above the other curves, for their $\sigma_{\text{ann}} v$ are of order $\mathcal{O}(v^2)$. And we note that there are downward bends in the upper bound curves at about $M_\chi \sim m_t = 171.2$ GeV account for the $\chi \bar{\chi} \rightarrow t \bar{t}$ threshold effect.

VI. VALIDITY REGION OF EFFECTIVE MODELS AND COMBINED CONSTRAINTS

In this section, let us discuss the validity region where the method of effective theory can be used. For a generic 4-fermion interaction operator $\frac{G_f}{\sqrt{2}} \bar{\chi} \Gamma_1 \chi \bar{f} \Gamma_2 f$, the mass dimension of the coupling G_f is -2 . Since we have used the two types of coupling constants, i.e., the universal couplings and the Yukawa-like couplings ($G_f \propto m_f$), in the numerical calculation throughout the last three sections, let us consider them case by case:

- For the universal couplings, we can write the coupling as $\frac{G_f}{\sqrt{2}} = \frac{\alpha}{\Lambda^2}$, where Λ is the cutoff energy scale and α is the coupling of the fundamental theory beyond Λ , which may be of order 1. The transfer momentum of the annihilation process $\chi \bar{\chi} \rightarrow f \bar{f}$ must be well below the cutoff, that is, $2M_\chi \ll \Lambda$, so that the effective theory can be used. On the other hand, a weakly coupled UV completion of the effective theory usually requires $\alpha < 4\pi$ such that the perturbation can be adopted [41, 63]. From the above 3 relations, we obtain

$$G_f \ll \frac{\sqrt{2}\pi}{M_\chi^2} \quad (60)$$

- For the Yukawa-like couplings ($G_f \propto m_f$), we have $\frac{G_f}{\sqrt{2}} = \frac{\alpha m_f}{\Lambda^3}$, where Λ is a cutoff and α is of order 1. Likewise,

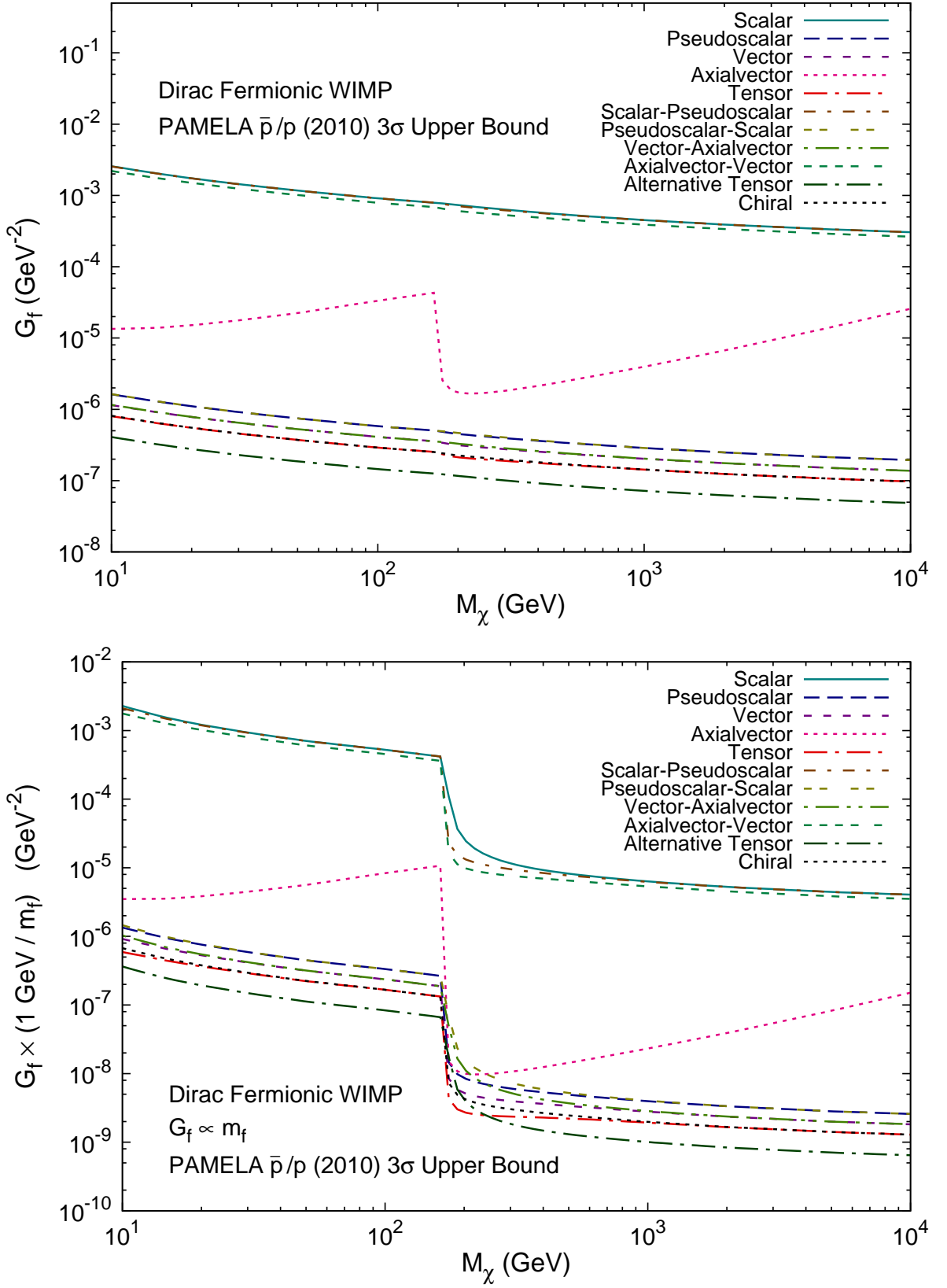


FIG. 6. The 3σ upper bounds on the coupling constants G_f from the PAMELA \bar{p}/p spectrum [58] in each effective model of 4-fermion interaction operators. In the upper frame, results are given for the case when the effective couplings to all the standard model fermions are equal (universal couplings). In the lower frame, results are shown for the case when the coupling constants are proportional to the fermion mass m_f .

we still have $2M_\chi \ll \Lambda$ and $\alpha < 4\pi$. From the above 3 relations, we obtain

$$\frac{G_f}{m_f} \ll \frac{\pi}{\sqrt{2}M_\chi^3} . \quad (61)$$

Eqs. (60) and (61) can be used to set the valid regions of the effective theories. Considering these validity conditions altogether with the other phenomenological constraints, we get the combined constraints on the effective models. In Figs. 7 – 14, we show the combined constraints on the coupling constants G_f of Dirac fermionic WIMPs with scalar (S), pseudoscalar (P), vector (V), axialvector (A), tensor (T), axialvector-vector (AV), alternative tensor (\tilde{T}), and chiral (C) interactions, respectively. The constraints for the pseudoscalar-scalar (PS) interactions are nearly the same as those for the P interactions. The constraints for the scalar-pseudoscalar (SP) and vector-axialvector (VA) interactions are nearly the same as those for the S and V interactions, respectively, except for that SP and VA interactions are insensitive to direct detection experiments. Note that only the effective models of the S, V, A, T, and C interactions suffer constraints from direct detection experiments. The SI constraints on the S, V and C interactions are much more stringent than the SD constraints on the A and T interactions.

From these figures, we can get interesting results. For the scalar and vector interactions that induce SI scattering with nuclei, the constraints from direct detection can be much stronger than the other constraints for the universal couplings, but weaker if the coupling is Yukawa-like. This is easily understood by considering the relation of DM-nucleon coupling constants and the DM-quark coupling constants given in Sec. IV. But for the axialvector and tensor operators that induce the SD interaction with nuclei we note that the direct detection constraints are much weaker than the indirect \bar{p}/p and relic density constraints. Further, we also note that in several cases the \bar{p}/p constraints can be stronger than the relic density constraints for DM mass lighter than 100 GeV. If the direct or indirect detection constraints are stronger than relic density, the constraints on the effective coupling are so weak that the thermal production may overclose the universe. Therefore the DM models in such cases should be excluded, or else some exotic entropy generation process should occur after DM freeze out.

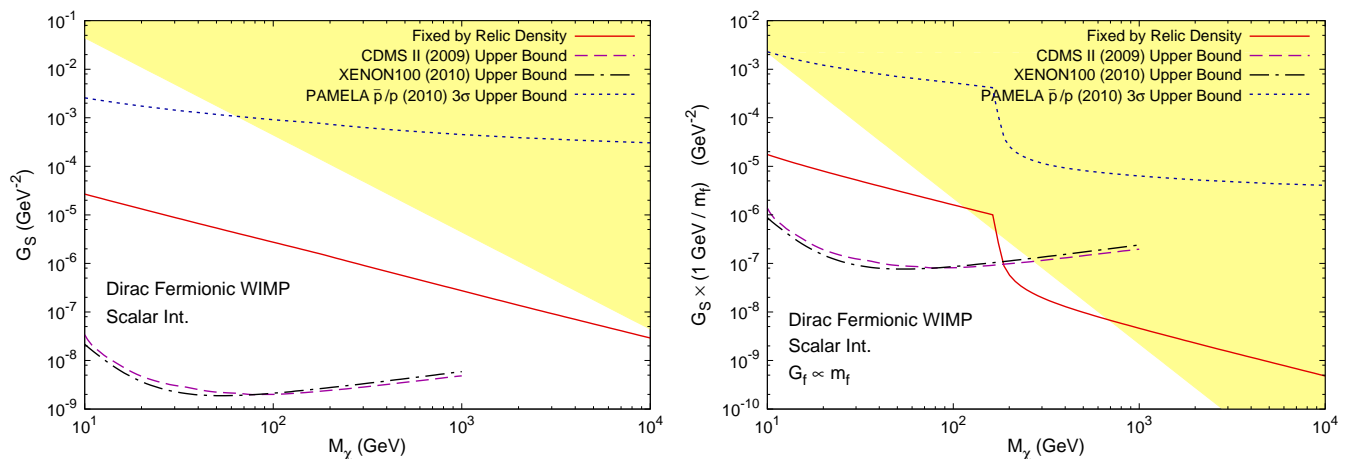


FIG. 7. Combined constraints on coupling constants G_f of Dirac fermionic WIMPs with scalar (S) interactions from relic density, direct detection experiments of CDMS II and XENON100, PAMELA \bar{p}/p ratio, and validity of effective theory. The yellow region denotes invalid parameter space of effective field theory. The left frame is shown for the case of universal couplings, while the right frame for the case of Yukawa-like couplings ($G_f \propto m_f$). The constraints for scalar-pseudoscalar (SP) interactions from relic density, PAMELA \bar{p}/p ratio, and validity of effective theory are nearly the same as above, but SP interactions are insensitive to direct detection experiments.

VII. CONCLUSION

In this work we give a general analysis of the 4-fermion interaction between the DM and the standard model particles. We have considered the most general form of the 4-fermion operators and corrected some errors in the previous works. We find that the constraints from DM relic density, DM direct detection and indirect detection of \bar{p}/p data are complementary to each other. Generally, the SI constraints are the most stringent while the SD constraints are quite weak. For light DM ($\lesssim 70$ GeV) the \bar{p}/p data give very strong constraints on the interaction.

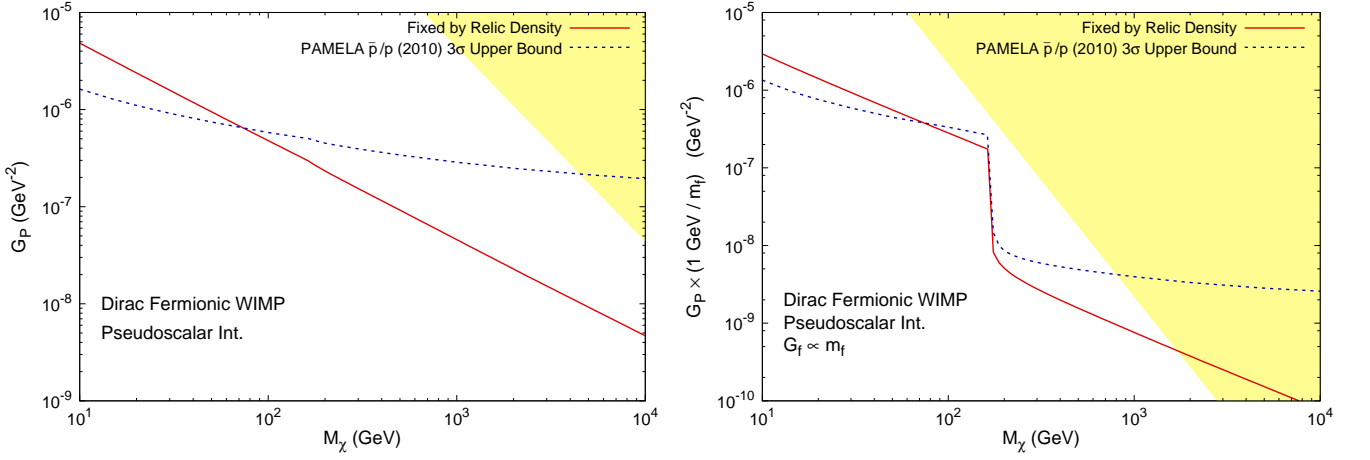


FIG. 8. Combined constraints on coupling constants G_f of Dirac fermionic WIMPs with pseudoscalar (P) interactions from relic density, PAMELA \bar{p}/p ratio, and validity of effective theory. The constraints for pseudoscalar-scalar (PS) interactions from relic density, PAMELA \bar{p}/p ratio, and validity of effective theory are nearly the same as above.

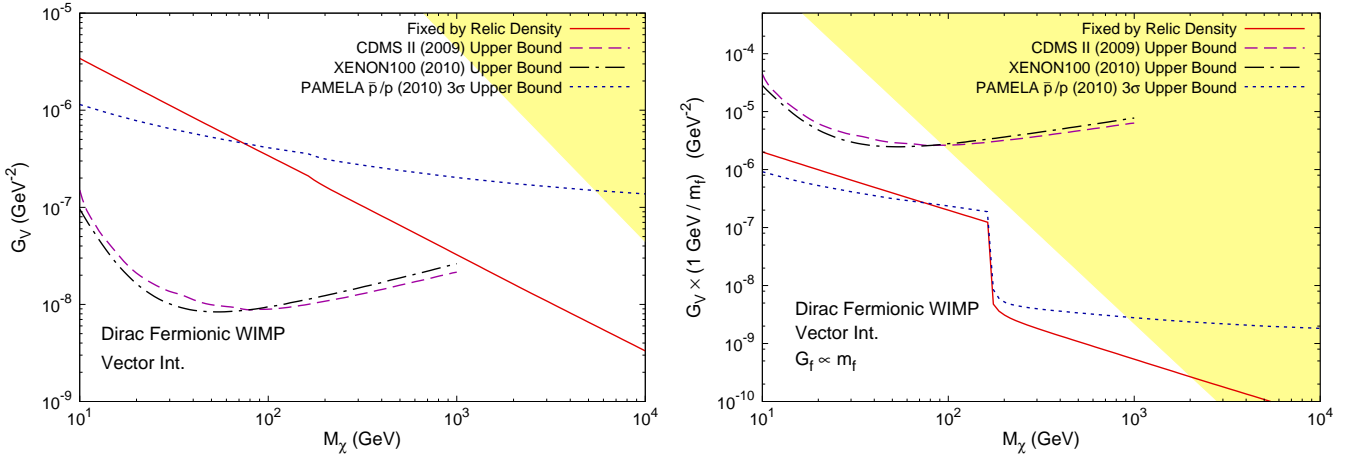


FIG. 9. Combined constraints on coupling constants G_f of Dirac fermionic WIMPs with vector (V) interactions from relic density, direct detection experiments of CDMS II and XENON100, PAMELA \bar{p}/p ratio, and validity of effective theory. The constraints for vector-axialvector (VA) interactions from relic density, PAMELA \bar{p}/p ratio, and validity of effective theory are nearly the same as above, but VA interactions are insensitive to direct detection experiments.

Assuming that one operator dominates the effective interaction between DM and the SM fermions, we find that some cases get so strong constraints that the universe will be overclosed by DM thermal production. In such cases the DM models are actually excluded assuming a standard cosmology. As a summary, in Tab. II, we indicate the excluded regions of M_χ given by direct and indirect experiments for Dirac fermionic WIMPs with various effective interactions. We find that recent direct detection experiments only exclude some regions of M_χ for the scalar, vector and chiral interactions with universal couplings, and for the scalar interaction with $G_f \propto m_f$. The PAMELA \bar{p}/p spectrum, however, excludes some small M_χ regions ($\lesssim 70$ GeV) for most of the effective interactions.

ACKNOWLEDGMENTS

This work is supported by the 973 project under Grant No. 2010CB833000, the National Natural Science Foundation of China (NSFC) under Grant Nos. 10773011, 11005163 and 11075169, the Specialized Research Fund for the Doctoral Program of Higher Education (SRFDP) under Grant No. 200805581030, the Fundamental Research Funds for the

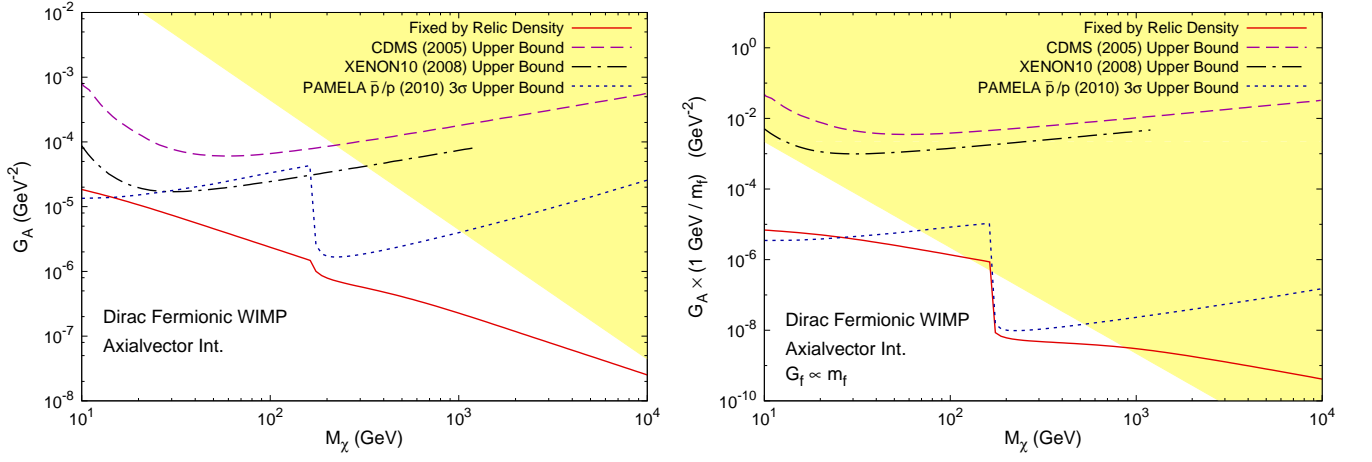


FIG. 10. Combined constraints on coupling constants G_f of Dirac fermionic WIMPs with axialvector (A) interactions from relic density, direct detection experiments of CDMS and XENON10, PAMELA \bar{p}/p ratio, and validity of effective theory.

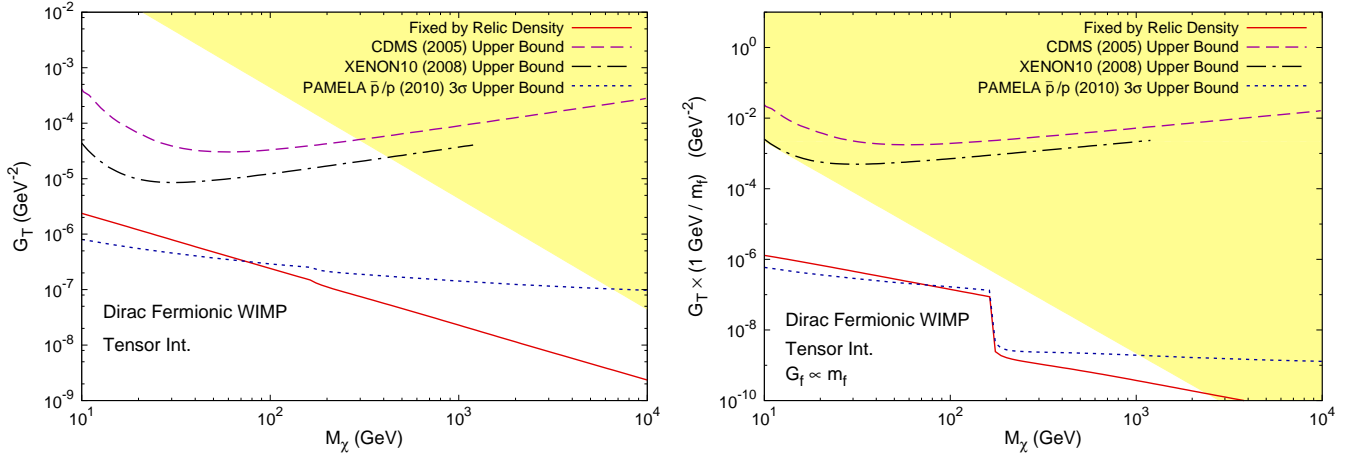


FIG. 11. Combined constraints on coupling constants G_f of Dirac fermionic WIMPs with tensor (T) interactions from relic density, direct detection experiments of CDMS and XENON10, PAMELA \bar{p}/p ratio, and validity of effective theory.

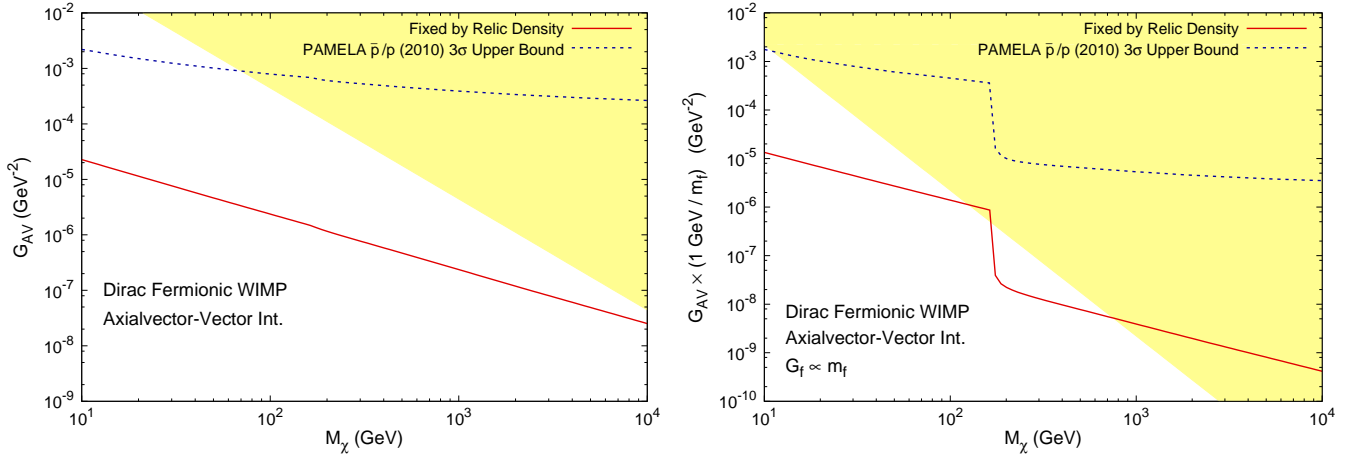


FIG. 12. Combined constraints on coupling constants G_f of Dirac fermionic WIMPs with axialvector-vector (AV) interactions from relic density, PAMELA \bar{p}/p ratio, and validity of effective theory.

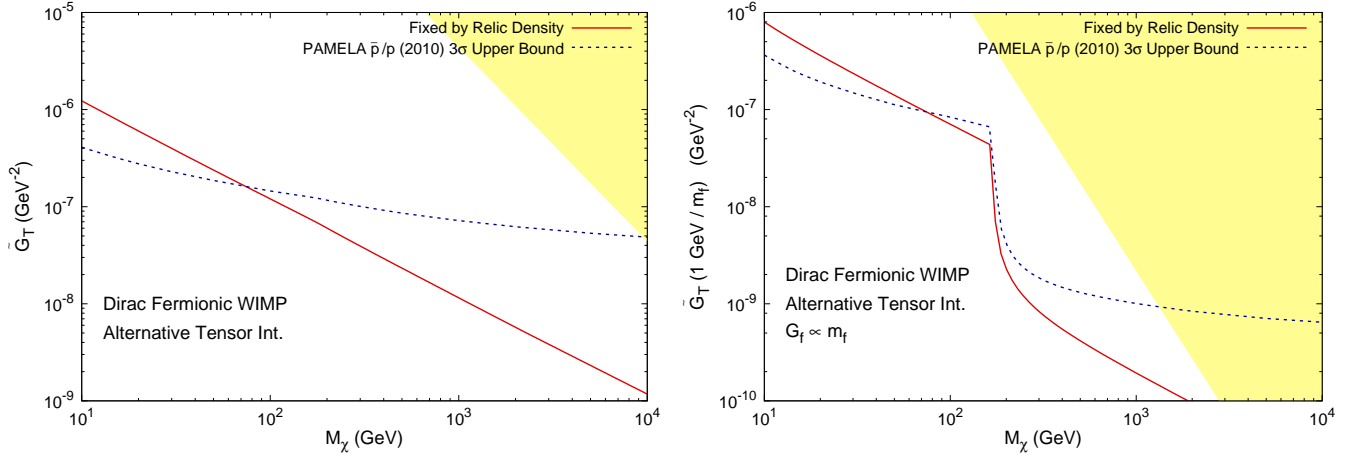


FIG. 13. Combined constraints on coupling constants G_f of Dirac fermionic WIMPs with alternative tensor (\tilde{T}) interactions from relic density, PAMELA \bar{p}/p ratio, and validity of effective theory.

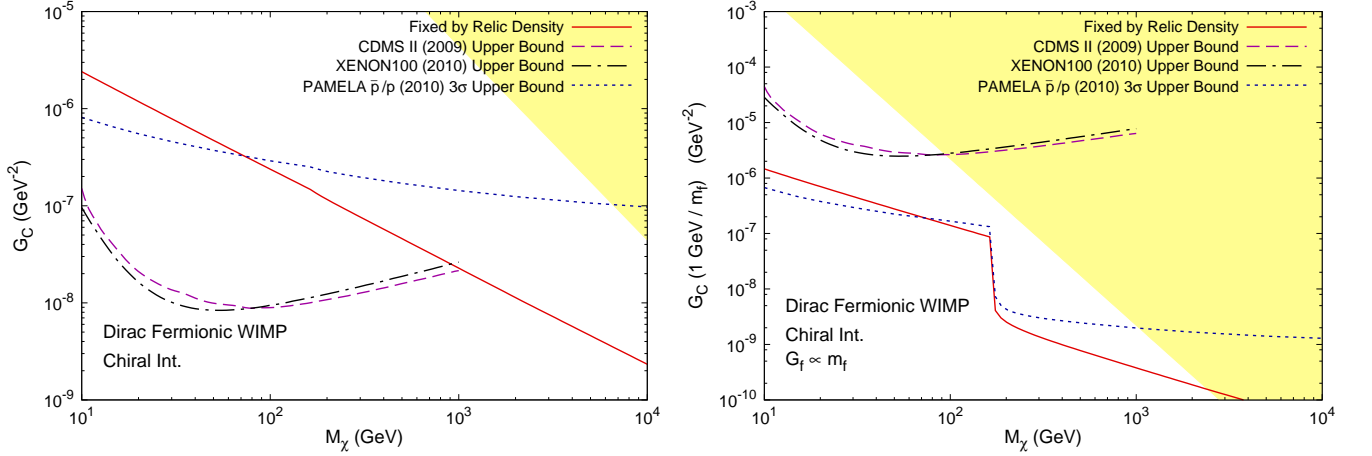


FIG. 14. Combined constraints on coupling constants G_f of Dirac fermionic WIMPs with chiral (C) interactions from relic density, direct detection experiments of CDMS II and XENON100, PAMELA \bar{p}/p ratio, and validity of effective theory.

Central Universities, and Sun Yat-Sen University Science Foundation.

-
- [1] M. Tegmark *et al.* [SDSS Collaboration], Phys. Rev. D **74**, 123507 (2006) [arXiv:astro-ph/0608632].
[2] E. Komatsu *et al.* [WMAP Collaboration], Astrophys. J. Suppl. **180**, 330 (2009) [arXiv:0803.0547 [astro-ph]].
[3] E. Komatsu *et al.*, arXiv:1001.4538 [astro-ph.CO].
[4] E. W. Kolb and M. S. Turner, *The Early Universe* (Westview, Boulder, 1994).
[5] G. Jungman, M. Kamionkowski and K. Griest, Phys. Rept. **267**, 195 (1996) [arXiv:hep-ph/9506380].
[6] G. Bertone, D. Hooper and J. Silk, Phys. Rept. **405**, 279 (2005) [arXiv:hep-ph/0404175]. D. Hooper, arXiv:0901.4090 [hep-ph].
[7] H. Murayama, arXiv:0704.2276 [hep-ph].
[8] J. L. Feng, arXiv:1003.0904 [astro-ph.CO].
[9] H. Goldberg, Phys. Rev. Lett. **50**, 1419 (1983) [Erratum-ibid. **103**, 099905 (2009)].
[10] J. R. Ellis, J. S. Hagelin, D. V. Nanopoulos, K. A. Olive and M. Srednicki, Nucl. Phys. B **238**, 453 (1984).
[11] G. L. Kane, C. F. Kolda, L. Roszkowski and J. D. Wells, Phys. Rev. D **49**, 6173 (1994) [arXiv:hep-ph/9312272].
[12] E. W. Kolb and R. Slansky, Phys. Lett. B **135**, 378 (1984).
[13] H. C. Cheng, J. L. Feng and K. T. Matchev, Phys. Rev. Lett. **89**, 211301 (2002) [arXiv:hep-ph/0207125].
[14] D. Hooper and S. Profumo, Phys. Rept. **453**, 29 (2007) [arXiv:hep-ph/0701197].

TABLE II. A summary for Dirac fermionic WIMPs with various effective interactions. The excluded regions of M_χ given by direct and indirect experiments are indicated.

Universal coupling		
Interaction	Direct detection	PAMELA \bar{p}/p
Scalar	Excluded $M_\chi \simeq 10$ GeV – above 1 TeV	Not sensitive
Pseudoscalar	Not sensitive	Excluded $M_\chi \simeq 10 - 70$ GeV
Vector	Excluded $M_\chi \simeq 10$ GeV – 1 TeV	Excluded $M_\chi \simeq 10 - 70$ GeV
Axialvector	Not sensitive	Excluded $M_\chi \simeq 10 - 14$ GeV
Tensor	Not sensitive	Excluded $M_\chi \simeq 10 - 70$ GeV
Scalar-pseudoscalar	Not sensitive	Not sensitive
Pseudoscalar-scalar	Not sensitive	Excluded $M_\chi \simeq 10 - 70$ GeV
Vector-axialvector	Not sensitive	Excluded $M_\chi \simeq 10 - 70$ GeV
Axialvector-vector	Not sensitive	Not sensitive
Alternative tensor	Not sensitive	Excluded $M_\chi \simeq 10 - 70$ GeV
Chiral	Excluded $M_\chi \simeq 10$ GeV – 1 TeV	Excluded $M_\chi \simeq 10 - 70$ GeV
$G_f \propto m_f$		
Interaction	Direct detection	PAMELA \bar{p}/p
Scalar	Excluded $M_\chi \simeq 10 - 185$ GeV	Not sensitive
Pseudoscalar	Not sensitive	Excluded $M_\chi \simeq 10 - 70$ GeV
Vector	Not sensitive	Excluded $M_\chi \simeq 10 - 70$ GeV
Axialvector	Not sensitive	Excluded $M_\chi \simeq 10 - 25$ GeV
Tensor	Not sensitive	Excluded $M_\chi \simeq 10 - 70$ GeV
Scalar-pseudoscalar	Not sensitive	Not sensitive
Pseudoscalar-scalar	Not sensitive	Excluded $M_\chi \simeq 10 - 70$ GeV
Vector-axialvector	Not sensitive	Excluded $M_\chi \simeq 10 - 70$ GeV
Axialvector-vector	Not sensitive	Not sensitive
Alternative tensor	Not sensitive	Excluded $M_\chi \simeq 10 - 70$ GeV
Chiral	Not sensitive	Excluded $M_\chi \simeq 10 - 68$ GeV

- [15] G. Servant and T. M. P. Tait, Nucl. Phys. B **650**, 391 (2003) [arXiv:hep-ph/0206071].
[16] G. Servant and T. M. P. Tait, New J. Phys. **4**, 99 (2002) [arXiv:hep-ph/0209262].
[17] K. Agashe and G. Servant, Phys. Rev. Lett. **93**, 231805 (2004) [arXiv:hep-ph/0403143].
[18] K. Agashe and G. Servant, JCAP **0502**, 002 (2005) [arXiv:hep-ph/0411254].
[19] K. Agashe, A. Falkowski, I. Low and G. Servant, JHEP **0804**, 027 (2008) [arXiv:0712.2455 [hep-ph]].
[20] H. C. Cheng and I. Low, JHEP **0408**, 061 (2004) [arXiv:hep-ph/0405243].
[21] I. Low, JHEP **0410**, 067 (2004) [arXiv:hep-ph/0409025].
[22] A. Birkedal, A. Noble, M. Perelstein and A. Spray, Phys. Rev. D **74**, 035002 (2006) [arXiv:hep-ph/0603077].
[23] A. Freitas, P. Schwaller and D. Wyler, JHEP **0912**, 027 (2009) [arXiv:0906.1816 [hep-ph]].
[24] C. S. Kim and J. Park, Phys. Lett. B **688**, 323 (2010) [arXiv:0911.2389 [hep-ph]].
[25] E. M. Dolle and S. Su, Phys. Rev. D **77**, 075013 (2008) [arXiv:0712.1234 [hep-ph]].
[26] W. L. Guo, L. M. Wang, Y. L. Wu and C. Zhuang, Phys. Rev. D **78**, 035015 (2008) [arXiv:0805.0401 [hep-ph]].
[27] W. L. Guo, L. M. Wang, Y. L. Wu, Y. F. Zhou and C. Zhuang, Phys. Rev. D **79**, 055015 (2009) [arXiv:0811.2556 [hep-ph]].
[28] W. L. Guo, Y. L. Wu and Y. F. Zhou, Phys. Rev. D **81**, 075014 (2010) [arXiv:1001.0307 [hep-ph]].
[29] A. Birkedal, K. Matchev and M. Perelstein, Phys. Rev. D **70**, 077701 (2004) [arXiv:hep-ph/0403004].
[30] F. Giuliani, Phys. Rev. Lett. **93**, 161301 (2004) [arXiv:hep-ph/0404010].
[31] A. Kurylov and M. Kamionkowski, Phys. Rev. D **69**, 063503 (2004) [arXiv:hep-ph/0307185].
[32] M. Beltran, D. Hooper, E. W. Kolb and Z. C. Krusberg, Phys. Rev. D **80**, 043509 (2009) [arXiv:0808.3384 [hep-ph]].
[33] M. Cirelli, M. Kadastik, M. Raidal and A. Strumia, Nucl. Phys. B **813**, 1 (2009) [arXiv:0809.2409 [hep-ph]].
[34] W. Shepherd, T. M. P. Tait and G. Zaharijas, Phys. Rev. D **79**, 055022 (2009) [arXiv:0901.2125 [hep-ph]].
[35] Q. H. Cao, I. Low and G. Shaughnessy, Phys. Lett. B **691**, 73 (2010) [arXiv:0912.4510 [hep-ph]].
[36] Q. H. Cao, C. R. Chen, C. S. Li and H. Zhang, arXiv:0912.4511 [hep-ph].
[37] M. Beltran, D. Hooper, E. W. Kolb, Z. A. C. Krusberg and T. M. P. Tait, JHEP **1009**, 037 (2010) [arXiv:1002.4137]

- [hep-ph]].
- [38] A. L. Fitzpatrick, D. Hooper and K. M. Zurek, Phys. Rev. D **81**, 115005 (2010) [arXiv:1003.0014 [hep-ph]].
 - [39] J. Goodman, M. Ibe, A. Rajaraman, W. Shepherd, T. M. P. Tait and H. B. P. Yu, arXiv:1005.1286 [hep-ph].
 - [40] Y. Bai, P. J. Fox and R. Harnik, arXiv:1005.3797 [hep-ph].
 - [41] J. Goodman, M. Ibe, A. Rajaraman, W. Shepherd, T. M. P. Tait and H. B. P. Yu, arXiv:1008.1783 [hep-ph].
 - [42] J. Goodman, M. Ibe, A. Rajaraman, W. Shepherd, T. M. P. Tait and H. B. P. Yu, arXiv:1009.0008 [hep-ph].
 - [43] N. F. Bell, J. B. Dent, T. D. Jacques and T. J. Weiler, arXiv:1009.2584 [hep-ph].
 - [44] Z. Ahmed *et al.* [The CDMS-II Collaboration], Science **327**, 1619 (2010) [arXiv:0912.3592 [astro-ph.CO]].
 - [45] E. Aprile *et al.* [XENON100 Collaboration], Phys. Rev. Lett. **105**, 131302 (2010) [arXiv:1005.0380 [astro-ph.CO]].
 - [46] D. S. Akerib *et al.* [CDMS Collaboration], Phys. Rev. D **73**, 011102 (2006) [arXiv:astro-ph/0509269].
 - [47] J. Angle *et al.* [XENON10 Collaboration], Phys. Rev. Lett. **101**, 091301 (2008) [arXiv:0805.2939 [astro-ph]].
 - [48] M. Srednicki, R. Watkins and K. A. Olive, Nucl. Phys. B **310**, 693 (1988).
 - [49] P. Gondolo and G. Gelmini, Nucl. Phys. B **360**, 145 (1991).
 - [50] J. C. Mather, D. J. Fixsen, R. A. Shafer, C. Mosier and D. T. Wilkinson, Astrophys. J. **512**, 511 (1999) [arXiv:astro-ph/9810373].
 - [51] T. S. Coleman and M. Roos, Phys. Rev. D **68**, 027702 (2003) [arXiv:astro-ph/0304281].
 - [52] P. Agrawal, Z. Chacko, C. Kilic and R. K. Mishra, arXiv:1003.1912 [hep-ph].
 - [53] J. R. Ellis, A. Ferstl and K. A. Olive, Phys. Lett. B **481**, 304 (2000) [arXiv:hep-ph/0001005].
 - [54] G. Belanger, F. Boudjema, A. Pukhov and A. Semenov, Comput. Phys. Commun. **180**, 747 (2009) [arXiv:0803.2360 [hep-ph]].
 - [55] A. Airapetian *et al.* [HERMES Collaboration], Phys. Rev. D **75**, 012007 (2007) [arXiv:hep-ex/0609039].
 - [56] A. W. Strong and I. V. Moskalenko, Astrophys. J. **509**, 212 (1998) [arXiv:astro-ph/9807150].
 - [57] A. W. Strong and I. V. Moskalenko, arXiv:astro-ph/9906228.
 - [58] O. Adriani *et al.* [PAMELA Collaboration], Phys. Rev. Lett. **105**, 121101 (2010) [arXiv:1007.0821 [astro-ph.HE]].
 - [59] T. Sjostrand, S. Mrenna and P. Z. Skands, JHEP **0605**, 026 (2006) [arXiv:hep-ph/0603175].
 - [60] J. F. Navarro, C. S. Frenk and S. D. M. White, Astrophys. J. **490**, 493 (1997) [arXiv:astro-ph/9611107].
 - [61] R. Catena and P. Ullio, JCAP **1008**, 004 (2010) [arXiv:0907.0018 [astro-ph.CO]].
 - [62] P. Salucci, F. Nesti, G. Gentile and C. F. Martins, arXiv:1003.3101 [astro-ph.GA].
 - [63] X. J. Bi, R. Brandenberger, P. Gondolo, T. j. Li, Q. Yuan and X. m. Zhang, Phys. Rev. D **80**, 103502 (2009) [arXiv:0905.1253 [hep-ph]].